Superoxide and hydroxyl radicals contribute to gyrase inhibitor-mediated cell death in *Escherichia coli*

Daniel J. Dwyer*, Michael A. Kohanski*, Boris Hayete and James J. Collins

* These authors contributed equally to this work

Supplementary Results

Engineered riboregulation effectively represses and efficiently activates CcdB expression *in vivo*

To determine the *in vivo* effect of overexpression of the F-plasmid encoded toxin CcdB, we amplified the *ccdB* gene and coupled it to a previously described plasmid-borne expression system that enables precise control of gene expression through highly specific RNA-RNA interactions (Isaacs et al., 2004). This system, referred to as engineered riboregulation, has been shown to repress mRNA expression *in vivo* by 98% due to designed secondary structure formation, thus providing much tighter control than that of commonly used inducible promoters (*ccdB* expression plasmids lacking the *cis*-repressive sequence could not be transformed). This secondary structure, a stem loop, serves as a binding target for a non-coding RNA (ncRNA), expressed in *trans*, that interacts with high specificity for systematic activation of translation via alleviation of the mRNA's *cis*-repressive secondary structure. The engineered riboregulation system employs independent IPTG-inducible (LacI operator site containing) modified lambda pL (Lutz and Bujard, 1997) and arabinose-inducible *araBAD* promoters for the transcription of *cis*-repressed mRNA and *trans*-activating ncRNA, respectively.

Activation of the *araBAD* promoter requires binding of AraC. However, the *araC* gene has been deleted in BW25113 cells. To overcome this hurdle, we amplified the endogenous *araC* promoter and the *araC* gene. These elements were then subcloned onto our CcdB riboregulation plasmid.

Identification and functional enrichment of significantly changing genes in response to gyrase inhibition

All genes have a natural expression range which, under typical conditions, is not fully explored. Even when a gene's dynamic range is well-explored by experiments, a certain expression state will usually dominate. In order to achieve consistency between microarrays, we normalized our data, in conjunction with the M^{3D} compendium (T. Gardner, Boston University, http://m3d.bu.edu) using the RMA method of normalization (Irizarry et al., 2003). This resulted in a log-scale microarray compendium of >600 chips. We approximated each genes fluctuation around its respective compendium mean with a gaussian model, where each expression value was replaced with the corresponding z-score around that gene's mean. Finally, for each point of the time-series, we computed the z-score difference between the gyrase-inhibitor treatment and the untreated control, allowing us to analyze the change of expression of a gene in terms of the estimated standard deviation of that gene (Supplemental Table 1). The standard deviation of any gene in the compendium had to be biased by the experimental conditions of which the compendium is comprised. Nevertheless, we found the standard deviation interval to be a robust representation of the difference of expression even for biased genes, e.g. for LexA, which was heavily perturbed in the compendium. More importantly, this measure was designed to be independent of a gene's dynamic range and sensitive to the statistical significance of a change of expression between the treatment and control. This allowed us to eliminate genes that change similarly over time in both a gyrase-inhibitor treatment and the control expression sets, and to focus on genes that change expression levels specifically as a function of the treatment using a robust statistical measure as our thresholding parameter. In this regard, it was preferable to the more usual log-ratio metric, which forces the choice of an arbitrary significance threshold independent of a gene's dynamic range.

Following the detection of the significantly changing genes at each timepoint, we performed functional enrichment using Gene Ontology classification (Ashburner et al., 2000; Camon et al., 2004), and the program GO::TermFinder (Boyle et al., 2004), in order to track temporal gene expression changes (Supplementary Figures 1 and 2, Supplementary Table 2).. Functional enrichment was performed under the hypergeometric model of random occurrence. In order to simplify the gene expression

picture, we reduced the set of differentially expressing genes to the responsible transcription factors in the following manner. First, for each gene in the set of significantly changed genes we determined its transcription factor in RegulonDB 5.0 (Salgado et al., 2006). Then, starting with the most-represented regulator, we removed every gene regulated by a given transcription factor from the set of significantly changed genes, until no genes remained, or until none of the remaining genes had a known transcription factor. We used the resultant set of transcription factors as an approximation of the transcriptional program differentially expressed between gyrase inhibitor treated and untreated cultures.

In addition, we determined statistical enrichment of transcription factors' individual regulons at every time point (Supplementary Table 3). To this end, we restricted the list of differentially expressed genes, constructed as described above, to only those genes whose regulation was described in RegulonDB and a recently published set of regulatory connections (Faith et al., 2007). For each transcription factor both databases, we calculated the likelihood of finding the given number of its targets in this reduced query set using hypergeometric distribution, under the assumption that each transcription factor's regulon was correctly and completely described by RegulonDB and the regulation map. Finally, as a separate analysis of differential gene expression, we conflated difference of z-scores across all time points by utilizing the formula, Zaverage = sum_t (Z_t)/sqrt(t) (Whitlock, 2005) (Figure 2).

Phenotypic analysis of deletion mutants

To identify potential gyrase inhibitor-mediated genetic responses that contribute to cellular death in *E. coli*, we screened single-gene knockout strains from a BW25113 deletion library (Baba et al., 2006). Knockout strains were selected based on our microarray functional enrichment results, and we monitored changes in survival (relative to wildtype cells) upon norfloxacin exposure or CcdB expression. We analyzed a subset of genes involved in DNA damage sensing, ATP synthesis, oxidative stress response, Fe-S cluster synthesis and global iron regulation to better understand how these biochemical processes affect the ability of *E. coli* to survive gyrase poisoning (Supplemetary Figure 7).

We first used a *recA* deletion strain to examine how the inability to sense DNA damage and initiate the SOS response via RecA would affect cell survival. We observed a drastic 4-log reduction in cell survival in the first hour after application of norfloxacin, and an additional 1-log reduction over the remainder of the experiment. Given these data, the severe reaction of Δ*recA* cells treated with norfloxacin suggests that quinolone treatment of these SOS-compromised cells is overwhelming and appears to rapidly breakdown cellular functionality. We observed a similarly strong, near 3-log reduction in viability in the first hour following induction of CcdB expression. Together, these results highlight how rapidly DNA damage occurs following norfloxacin- and CcdB-mediated gyrase inhibition.

In light of the observed downregulated expression of anaerobic respiratory components and upregulation of ATP synthase component genes, we hypothesized that gyrase inhibitor-mediated supercoiling changes lead to a burst in superoxide formation owed to increased respiratory chain activity. We challenged the majority of ATP synthase component genes with norfloxacin and observed increased survival in each case. Our norfloxacin results demonstrate that efficient killing is directly dependent on ATP, supporting published *in vitro* and *in vivo* findings (Kampranis and Maxwell, 1998; Li and Liu, 1998). Further, these results are consistent with previous work (Deitz et al., 1966; Li and Liu, 1998), in which chemical uncoupling of oxidative phosphorylation prevented DNA damage following quinolone poisoning of gyrase.

We next examined the effect of gyrase inhibition on a *sodB* deletion strain. While Δ*sodB* and wildtype cells treated with norfloxacin showed similar growth behavior between the 0 and 2 hour time points, Δ*sodB* cells exhibited decreased survival over the final four hours of the experiment. The delay in the phenotypic response to norfloxacin treatment in this strain implies that superoxide generation and accumulation does not occur immediately following DNA damage formation, and is consistent with the steps in our oxidative damage cell death pathway model. Expression of CcdB in Δ*sodB* cells similarly resulted in decreased survival when compared to wildtype. Together, these data suggest that SodB-related protection of Fe-S cluster proteins from superoxide damage is an important factor in the survival of gyrase-poisoned bacteria.

We then aimed to determine the role played by Fur, in cell survival following gyrase inhibition. Interestingly, we found that a *fur* deletion mutant responds slower and survives better than wildtype when challenged with norfloxacin. In contrast, wildtype and Δ*fur* cells expressing CcdB respond similarly over the first 3 hours of our experiments, yet do not exhibit the same ability to recover from gyrase poisoning and DNA damage formation. Relative to previous findings, in which exogenous iron import has been implicated in oxidative damage-mediated cell killing following exposure to hydrogen peroxide (Touati et al., 1995), our results imply that internal misregulation of iron is a critical factor in gyrase inhibitor-mediated cell death. This hypothesis was validated by our findings in Δ*tonB* cells. We observed no change in cellular viability following gyrase inhibiton by CcdB and norfloxacin in Δ*tonB* cells.

Considering that expression of *soxS* is stimulated by superoxide-mediated oxidative damage to the Fe-S cluster of its transcription factor, SoxR, we next studied whether impairment of Fe-S cluster synthesis affects cell killing by gyrase inhibition. We tested single knockouts of Fe-S cluster synthesis operon genes, *iscRSUA*. Δ*iscR*, Δ*iscU* and Δ*iscA* deletion mutants all responded to application of norfloxacin in a manner similar to wildtype cultures. We also tested the phenotypic effect of norfloxacin addition on Δ*sufS* cells and found that this strain also behaved like wildtype cells.

Lastly we monitored the effect on growth of norfloxacin treatment in both Δ*soxS* and Δ*sodA* backgrounds. We found that both deletion strains behaved comparably to norfloxacin-treated wildtype cells.

RecA, SoxS and Fur response to gyrase inhibition

On the basis of our phenotypic and microarray results, we contend that gyrase inhibitor-mediated DNA damage promotes the formation of superoxide radicals. In turn, we propose that sustained oxidation of Fe-S clusters by superoxide results in the breakdown of iron regulatory dynamics. To monitor the occurrence of these biochemical events, we designed sensor constructs that activate green fluorescent protein (GFP) expression in response to DNA lesion formation, Fe-S cluster oxidation by superoxide, and derepression of iron-related genes, respectively. Measurement of GFP fluorescence

by flow cytometry allowed us to monitor population responses to norfloxacin treatment and CcdB expression at single-cell resolution (Supplementary Figure 6).

Our DNA damage sensor construct employs an engineered promoter that relies upon LexA repression for regulation of *gfp* transcription, and is thus sensitive to RecA-stimulated autocleavage following DNA lesion formation and recognition (Little, 1991). Gyrase poisoning of wildtype bacteria resulted in significant GFP expression from this sensor. To monitor Fe-S cluster oxidation, we placed *gfp* under the transcriptional control of the native *soxS* promoter to create an Fe-S cluster damage sensor; the *soxS* promoter is regulated by the redox state of the SoxR Fe-S cluster, and superoxide-triggered oxidation activates transcription (Hidalgo et al., 1998). Gyrase inhibition by either norfloxacin or CcdB resulted in GFP expression from this sensor, demonstrating that attack Fe-S clusters by superoxide is occurring and that superoxide attack is sustained. To determine if DNA and oxidative damage promote derepression of iron uptake and utilization genes, we constructed an iron regulation sensor construct that employs the transcription factor Fur as the mediator of *gfp* transcription. As sustained Fe-S cluster attack by superoxide should increase the intracellular concentration of "free iron", an increase in GFP expression would suggest that iron misregulation is occurring. Accordingly, following norfloxacin treatment and CcdB expression, respectively, we observed increased expression of GFP from our iron regulation sensor construct.

Given the phenotypic effect of genetic-level uncoupling of oxidative phosphorylation and impairment of Fe-S cluster repair by inhibiting *de novo* cluster synthesis on gyrase inhibitor-mediated cell death, we next monitored the DNA damage, oxidative damage and iron regulatory sensor responses in Δ*atpC* and Δ*iscS* cells, respectively. Genetic-level uncoupling of ATP synthase and reduced respiratory chain activity should significantly inhibit superoxide formation and Fe-S cluster-induced changes in iron regulation as a function of gyrase poisoning. Consistent with our model, gyrase inhibition by norfloxacin and CcdB, respectively, in Δ*atpC* cells resulted in negligible superoxide- and Fur-related GFP expression changes. We also observed intermediate levels of fluorescence from our DNA damage sensor, demonstrating that both modes of gyrase poisoning induce lesion formation in this strain, and indicating that

substrate-level phosphorylation generates enough ATP in Δ*atpC* cells to enable norfloxacin and CcdB lesion induction.

The ability to replenish Fe-S clusters damaged by superoxide plays a critical role in maintaining an available pool of ferrous iron for hydroxyl radical formation via Fenton chemistry. Consistent with this, we found that the application of norfloxacin to Δ*iscS* cells induced GFP expression from our DNA damage sensor at levels comparable to wildtype. The oxidative damage response exhibited a tighter fluorescence distribution than wildtype, suggesting that efficient turnover of Fe-S clusters is required for maximum induction of the *soxS* promoter. As expected, inhibition of Fe-S cluster turnover results in an intermediate level of GFP expression from our iron regulation sensor, indicating that Fe-S cluster integrity plays an important role in iron regulation. In CcdB-expressing Δ*iscS* cells, which exhibited the largest increase in survival with CcdB expression, we observed a lower, yet broad, level of fluorescence from our DNA damage sensor. This demonstrates that DNA breaks are introduced in this strain and may explain the slight reduction in CFU/mL between induced and uninduced Δ*iscS* cultures. Our oxidative damage sensor exhibited an intermediate fluorescence response, while our iron regulation sensor revealed that the large majority of Δ*iscS* cells poisoned by CcdB exhibited negligible changes in GFP expression. Both sets of sensor results are consistent with the hypothesis that the Δ*iscS* mutation results in decreased oxidative damage to Fe-S clusters. Further, these results highlight the important role of redox cycling in the breakdown of iron regulatory dynamics.

We also monitored the DNA damage, oxidative damage and iron regulatory responses in our Δ*fur*, Δ*recA* and Δ*sodB* strains. GFP expression levels from each sensor, in each strain, were consistent with our phenotypic results.

Time course sensor construct and hydroxyl radical response of wildtype to norfloxacin treatment

We monitored, via flow cytometry, gfp expression from our DNA damage sensor, Fur sensor, and iron-sulfur cluster damage sensor as well as hydroxyl radical formation every hour over a 6-hour treatment with 250ng/mL of norfloxacin (Supplementary Figure 9). In all cases, we see an increase in DNA damage, Fur derepression, iron-sulfur cluster damage, and hydroxyl radical formation over the first 3-hours of norfloxacin treatment

followed by stabilization of gfp expression and hydroxyl radical levels. The similar patterns of expression suggest a connection between iron homeostasis, iron-sulfur cluster stability, hydroxyl radical levels and DNA damage. The insets show untreated wildtype cultures followed with the sensor constructs and HPF dye, respectively, over the same time course. In all cases, we do not observe an increase in DNA damage, Fur derepression, iron-sulfur cluster damage, and hydroxyl radical levels as a function of growth alone.

Baseline responses (time zero) of BW25113 knockout strains to sensor constructs and hydroxyl radical levels

Time zero hours refers to the measurement immediately before norfloxacin treatment or CcdB expression. With our strains, both with and without the CcdB expression vector, we see little deviation from wildtype for our DNA damage sensor (Supplementary Figure 10) for all but Δ*fur* in the case of norfloxacin and the CcdB containing Δ*iscS*, both of which show a minimal increase. Similarly, all knockout strains harboring the CcdB expression vector show little deviation in at time zero for fur derepression or for iron-sulfur cluster damage. The norfloxacin treated strains show little deviation from wildtype at time zero for iron-sulfur cluster damage with the exception of Δ*fur*, which is strongly repressed relative to wildtype even at time zero, and Δ*iscS* which shows a small amount of cluster damage at time zero. Similarly, the norfloxacin treated strains show little deviation from wildtype at time zero for Fur regulation (Supplemental Fig. 3b) with the exception of Δ*atpC*, which is more repressed than wildtype. At time zero, we see negligible changes in hydroxyl radical formation for the BW25113 strains, both with (Supplemental Fig. 4a)and without CcdB.

Gyrase poisoning and hydroxyl radical formation

In the Fenton reaction, free ferrous iron reacts with hydrogen peroxide to generate highly destructive hydroxyl radicals (Imlay, 2003). In our model, production of hydroxyl radicals is the cytotoxic end-product of redox cycling following a gyrase inhibitor-induced superoxide burst and Fe-S cluster damage. To detect the generation of hydroxyl radicals following gyrase inhibition by norfloxacin or CcdB, we employed the fluorescent

reporter dye, 3'-(p-hydroxyphenyl) fluorescein (HPF) (Setsukinai et al., 2003), which is oxidized by hydroxyl radicals with high specificity (Supplementary Figure 11).

As expected, we observed a significant increase in hydroxyl radical-induced fluorescence upon addition of norfloxacin to wildtype cells, the first direct demonstration of DNA gyrase inhibitor-induced hydroxyl radical generation. The largest detectable increase in fluorescence was observed in Δ*sodB* cells, while we did not detect hydroxyl radical production in Δ*atpC* cells. Additionally, Δ*iscS* cells expectedly exhibited a small increase in hydroxyl radical levels following norfloxacin treatment. We also observed decreased hydroxyl radical formation in Δ*fur* cells relative to wildtype, in line with the observed increase in Δ*fur* survival following application of norfloxacin. Interestingly, Δ*recA* cells treated with norfloxacin exhibited a small increase in hydroxyl radical formation. As all of our quinolone-related phenotypic Δ*recA* data suggest, norfloxacin induces DNA damage and cell death with remarkable efficiency in Δ*recA* cells. There is apparently little opportunity for cells to initiate our proposed oxidative damage cell death pathway if the treatment is this harsh. Accordingly, in the absence of RecA activity, a reduced concentration of hydroxyl radicals should still prove to greatly enhance the lethal effects of norfloxacin.

Expression of CcdB in wildtype cells likewise resulted in significant generation of hydroxyl radicals. Similar shifts in fluorescence values were detected in CcdB-expressing Δ*fur* and Δ*sodB* cells. While this is consistent with our survival results, it is unclear how the role of Fur is different with CcdB treatment in the context of iron misregulation and requires further investigation.

Similar to our norfloxacin results, CcdB expression in Δ*atpC* and Δ*iscS* cells yielded minimal changes in hydroxyl radical concentration. In contrast, we observed an increase in hydroxyl radical-related fluorescence in Δ*recA* cells, on par with fluorescence levels observed in CcdB+ wildtype cells. Our Δ*iscS* data shows that generation of hydroxyl radicals requires redox cycling, while our Δ*recA* data demonstrates that hydroxyl radical formation is an SOS-independent event.

Supplementary Materials and Methods

Plasmid construction, cell strains, and reagents

Basic molecular biology techniques were implemented as previously described (Sambrook and Russell, 2001). All plasmids were constructed using restriction endonucleases and T4 DNA Ligase from New England Biolabs (NEB, Beverly, MA). For cloning purposes, we transformed plasmids into the *E. coli* strain XL-10 (Stratagene, La Jolla, California; Tet^r Δ(mcrA)183, Δ(mcrCB-hsdSMR-mrr)173, endA1, supE44, thi-1, recA1, gyrA96, relA1, lac Hte [F proAB $lacI^q$ ZDM15 Tn10 (Tet^r) Amy Cam^r]) using standard heat-shock protocols (Sambrook and Russell, 2001). All cells were grown in selective medium: Luria-Bertani (LB) media (Fisher Scientific, Pittsburgh, PA) supplemented with 30 g/ml of kanamycin (Fisher Scientific). Plasmid isolation was performed using QIAprep Spin Miniprep Kits (Qiagen, Valencia, CA). Subcloning was confirmed by restriction analysis. Plasmid modifications were verified by sequencing, using the PE Biosystem ABI Prism 377 sequencer.

Our riboregulated CcdB expression plasmid was built according to our published design (Isaacs et al., 2004). The *ccdB* gene was amplified by PCR, from F plasmid-containing XL-10 cells, using the PTC-200 PCR machine (Bio-Rad, Waltham, MA) with the Expand Long Template PCR System (Roche, Indianapolis, IN). Oligonucleotide primers were purchased from Integrated DNA Technologies.

Briefly, transcription of *cis*-repressed *ccdB* mRNA was controlled using the $P_{LlacO-1}$ promoter (Lutz and Bujard, 1997), a modified version of the native bacteriophage λ P_L promoter containing two LacI operator sites; transcription was thus induced by addition of isopropyl-β-D-thiogalactopyranoside (IPTG, Fisher Scientific). The P_{BAD} promoter regulates the production of the *trans*-activating RNA necessary for CcdB toxin translation; CcdB translation was induced by addition of arabinose.

Our DNA damage and iron regulation sensors were based on the design of the $P_{LlacO-1}$ promoter (Lutz and Bujard, 1997). PCR was used to build each promoter, which employed LexA and Fur operator sites to regulate expression, respectively, of the green fluorescent protein gene, *gfpmut3b* (Cormack et al., 1996). To construct our oxidative

damage sensor, we PCR amplified the native *soxS* promoter from XL-10 cells and cloned it upstream of the *gfpmut3b* gene.

Phenotypic analysis

In our experiments, we compared the growth of untreated, norfloxacin treated (250ng/mL), CcdB- (uninduced cultures containing the *ccdB* riboregulator) and CcdB+ (induced cultures containing the *ccdB* riboregulator) wildtype BW25113 ($lacI^q$ $rrnB_{T14}$ $\Delta lacZ_{WJ16}$ *hsdR514* $\Delta araBAD_{AH33}$ $\Delta rhaBAD_{LD78}$;) cultures. In our specific single-gene knockout experiments, we studied the growth of deletion strains contained in a BW25113 deletion library (Baba et al., 2006).

For all experiments, cells were grown overnight, then were diluted 1:1,000 in 50mL LB (+30 g/ml kanamycin for CcdB expressing cells) for collection of OD_{600}, and colony forming unit (CFU/mL) samples. CcdB+ cultures were induced by addition of 1mM IPTG and 0.25% arabinose when cultures reached an OD_{600} of 0.3-0.4. Measurements of OD_{600} were taken using a SPECTRAFluor Plus (Tecan, Durham, NC). For CFU/mL measurements, 100 L of culture was collected, washed twice with filtered 1xPBS, pH 7.2 (Fisher Scientific), then serially diluted in 1xPBS. 10 L of each dilution was plated onto individual wells of a 24-well plate, with each well containing 1mL of LB-Agar (Fisher Scientific) (+30 g/ml kanamycin for CcdB expressing cells), and the plate incubated at 37°C overnight. Only dilutions that yielded between 20-100 colonies were counted, and CFU/mL values were calculated using the formula: [(#colonies)*(dilution factor)] / 0.01mL.

Gene expression analysis

We compared the microarray-determined mRNA profiles of *E. coli* BW25113 cultures in response to CcdB and norfloxacin, respectively, against untreated cultures. For all experiments, cells were grown overnight, then diluted 1:1,000 in 50mL LB (+30 g/ml kanamycin for CcdB-expressing cells) for collection of total RNA. CcdB-expressing cultures were induced with 1mM IPTG and 0.25% arabinose at an OD_{600} of 0.3-0.4; 250ng/mL norfloxacin was added to norfloxacin-treated cultures at an OD_{600} of 0.3-0.4. Untreated cultures were grown in LB with no exogenous inducers or antibiotics

added. Samples for microarray analysis were taken immediately before induction (time zero), then at 30, 60, and 120 minutes post induction.

Total RNA was obtained using the RNeasy Protect Bacteria Mini Kit (Qiagen) according to manufacturer's instructions. RNAprotect (Qiagen) was added to culture samples, which were then pelleted by centrifugation at 3000x*g* for 15 minutes and stored overnight at -80°C. Total RNA was then extracted using the RNeasy kit, and samples were DNase treated using DNA-*free* (Ambion, Austin, Tx). Sample concentration was estimated using the ND-1000 spectrophotometer (NanoDrop, Wilmington, Delaware).

cDNA was prepared from 10 μg total RNA through a random primed reverse transcription using SuperScript II (Invitrogen, Carlsbad, CA). The RNA was digested with the addition of 1M NaOH and incubation at 65ºC for 30 minutes. The mixture was neutralized with the addition of 1M HCl. The cDNA was purified using a QIAquick PCR purification column (Qiagen), following the manufacturer's protocol. The cDNA was fragmented to a size range of 50-200 bases with DNase I (0.6 U/ g cDNA) at 37 ºC for 10 minutes, followed by inactivation of the enzyme at 98 ºC for 10 minutes. Subsequently, the fragmented cDNA was biotin–labeled using an Enzo BioArray Terminal Labeling Kit with Biotin-ddUTP (Enzo Scientific, Farmingdale, NY). Fragmented, biotinylated cDNA was hybridized to Affymetrix E. Coli Antisense Genome arrays for 16 hours at 45 ºC and 60 rpm.

Following hybridization, arrays were washed and stained according to the standard Antibody Amplification for ProkaryoticTargets protocol (Affymetrix, Santa Clara, CA). This consisted of a wash with non–stringent buffer, followed by a wash with stringent buffer, a stain with Strepavidin, a wash with non-stringent buffer, a stain with biotinylated anti-strepavidin antibody, a stain with Strepavidin-Phycoerythrin, and a final wash with non-stringent buffer. The stained GeneChip arrays were scanned at 532 nm using an Affymetrix GeneChip Scanner 3000. The scanned images were scaled and quantified using GCOS v1.2 software.

The resulting *.CEL files were combined with *.CEL files from arrays which comprise the M3D compendium (T. Gardner, Boston University, http://m3d.bu.edu) and RMA-normalized (Irizarry et al., 2003), for a total of 505 RMA-normalized *E. coli* expression arrays. Subsequently, we subtracted the mean normalized expression for each

gene from its respective normalized expression for each individual experiment, and then divided by each gene by its respective standard deviation across all experiments. This converts the expression values for all genes across all experiments into estimated z-scores based upon the observed expression distribution for each gene across all experiments in the M3D compendium.

To determine statistically significant changes in gene expression due to norfloxacin treatment, or CcdB expression, we subtracted the expression z-score of each gene in our uninduced control dataset from the corresponding z-score in our perturbed (norfloxacin-treated or CcdB-expressing) sample dataset. This was done for each experimental time-point (0, 30, 60, 120, 180 minutes), e.g., the z-score of *recA* expression from our uninduced sample at 30 minutes was subtracted from the *recA* z-score from our norfloxacin-treated sample at 30 minutes. This allowed us to determine the difference in expression between an uninduced control set and a gyrase-inhibitor treated data set in terms of units of standard deviation, a robust metric. A gene was considered to have significantly changed expression when its z-score difference was greater than two units of standard deviation, with the sign determining over- and under-expression.

Following the identification of significantly changed genes at each time-point, we performed functional enrichment using the gene ontology (GO) classification system found on EcoCyc (Keseler et al., 2005). In doing this, we were able to group genes by GO annotated pathways. To track the changes in the cellular transcriptional program over time, we utilized the transcription factor regulatory information contained in RegulonDB (version 4) (Salgado et al., 2006). Using both sets of information, we were able to categorize significantly changed genes in functional units.

Sensor construct experiments using the flow cytometer

To monitor the occurrence of DNA damage, oxidative damage to Fe-S clusters and changes in iron regulation we employed our respective engineered sensors which respond to these biochemical events by activating expression of *gfpmut3b*. All data were collected using a Becton Dickinson FACSCalibur flow cytometer (Becton Dickinson, San Jose, CA) with a 488-nm argon laser and a 515- to 545-nm emission filter (FL1) at

low flow rate. The following PMT voltage settings were used: E00 (FSC), 300 (SSC), and 700 (FL1). Calibrite Beads (Becton Dickinson) were used for instrument calibration.

Flow data were converted to ASCII format using MFI (E. Martz, University of Massachusetts, Amherst), and processed with MATLAB (MathWorks, Natick, MA) to construct figures. At least 50,000 cells were collected for each sample

In all experiments, cells were grown overnight, then were diluted 1:1,000 in 50mL LB supplemented with 100 g /mL ampicillin (Fisher Scientific) (+30 g/ml kanamycin for CcdB expressing cells). CcdB expression was induced by addition of 1mM IPTG and 0.25% arabinose at an OD_{600} of 0.3-0.4, while 250ng/mL norfloxacin was added to drug treated cultures. Samples were taken immediately before induction (time zero), then every hour for 6 hours. At each timepoint, approximately 10^6 cells were collected, washed once and resuspended in filtered 1x PBS, pH 7.2 (Fisher Scientific), then measured on the flow cytometer.

Measurement of hydroxyl radicals using HPF dye

To detect hydroxyl radical formation following norfloxacin treatment or CcdB expression we used the fluorescent reporter dye, 3'-(p-hydroxyphenyl) fluorescein (HPF, Invitrogen), which is oxidized by hydroxyl radicals with high specificity. All data were collected using the Becton Dickinson FACSCalibur flow cytometer described above (Becton Dickinson). The following PMT voltage settings were used: E00 (FSC), 300 (SSC), and 825 (FL1). Calibrite Beads (Becton Dickinson) were used for instrument calibration. Flow data were collected, converted and analyzed as above.

In all experiments, cells were grown overnight, then were diluted 1:1,000 in 50mL LB (+30 g/ml kanamycin for CcdB expressing cells) supplemented with 5 M HPF. CcdB expression was induced by addition of 1mM IPTG and 0.25% arabinose at an OD_{600} of 0.3-0.4, while 250ng/mL norfloxacin was added to drug treated cultures. Samples were collected and prepared for flow cytometry as above.

Supplementary References

Ashburner, M., Ball, C.A., Blake, J.A., Botstein, D., Butler, H., Cherry, J.M., Davis, A.P., Dolinski, K., Dwight, S.S., Eppig, J.T., Harris, M.A., Hill, D.P., Issel-Tarver, L., Kasarskis, A., Lewis, S., Matese, J.C., Richardson, J.E., Ringwald, M., Rubin, G.M. and Sherlock, G. (2000) Gene ontology: tool for the unification of biology. The Gene Ontology Consortium. *Nat Genet*, **25**, 25-29.

Baba, T., Ara, T., Hasegawa, M., Takai, Y., Okumura, Y., Baba, M., Datsenko, K.A., Tomita, M., Wanner, B.L. and Mori, H. (2006) Construction of Escherichia coli K-12 in-frame, single-gene knockout mutants: the Keio collection. *Mol Syst Biol*, **2**, msb4100050-E4100051-msb4100050-E4100011.

Boyle, E.I., Weng, S., Gollub, J., Jin, H., Botstein, D., Cherry, J.M. and Sherlock, G. (2004) GO::TermFinder--open source software for accessing Gene Ontology information and finding significantly enriched Gene Ontology terms associated with a list of genes. *Bioinformatics*, **20**, 3710-3715.

Camon, E., Magrane, M., Barrell, D., Lee, V., Dimmer, E., Maslen, J., Binns, D., Harte, N., Lopez, R. and Apweiler, R. (2004) The Gene Ontology Annotation (GOA) Database: sharing knowledge in Uniprot with Gene Ontology. *Nucleic Acids Res*, **32**, D262-266.

Cormack, B.P., Valdivia, R.C. and Falkow, S. (1996) FACS-optimized mutants of the green fluorescent protein (GFP). *Gene*, **173**, 33-38.

Deitz, W.H., Cook, T.M. and Goss, W.A. (1966) Mechanism of action of nalidixic acid on Escherichia coli. 3. Conditions required for lethality. *J Bacteriol*, **91**, 768-773.

Faith, J.J., Hayete, B., Thaden, J.T., Mogno, I., Wierzbowski, J., Cottarel, G., Kasif, S., Collins, J. and Gardner, T. (2007) Large-scale mapping and validation of Escherichia coli transcriptional regulation from a compendium of expression profiles. *PLoS Biol*, **5**, e8.

Hidalgo, E., Leautaud, V. and Demple, B. (1998) The redox-regulated SoxR protein acts from a single DNA site as a repressor and an allosteric activator. *Embo J*, **17**, 2629-2636.

Imlay, J.A. (2003) Pathways of oxidative damage. *Annu Rev Microbiol*, **57**, 395-418.

Irizarry, R.A., Hobbs, B., Collin, F., Beazer-Barclay, Y.D., Antonellis, K.J., Scherf, U. and Speed, T.P. (2003) Exploration, normalization, and summaries of high density oligonucleotide array probe level data. *Biostatistics*, **4**, 249-264.

Isaacs, F.J., Dwyer, D.J., Ding, C., Pervouchine, D.D., Cantor, C.R. and Collins, J.J. (2004) Engineered riboregulators enable post-transcriptional control of gene expression. *Nat Biotechnol*, **22**, 841-847.

Kampranis, S.C. and Maxwell, A. (1998) The DNA gyrase-quinolone complex. ATP hydrolysis and the mechanism of DNA cleavage. *J Biol Chem*, **273**, 22615-22626.

Keseler, I.M., Collado-Vides, J., Gama-Castro, S., Ingraham, J., Paley, S., Paulsen, I.T., Peralta-Gil, M. and Karp, P.D. (2005) EcoCyc: a comprehensive database resource for Escherichia coli. *Nucleic Acids Res*, **33**, D334-337.

Li, T.K. and Liu, L.F. (1998) Modulation of gyrase-mediated DNA cleavage and cell killing by ATP. *Antimicrob Agents Chemother*, **42**, 1022-1027.

Little, J.W. (1991) Mechanism of specific LexA cleavage: autodigestion and the role of RecA coprotease. *Biochimie*, **73**, 411-421.

Lutz, R. and Bujard, H. (1997) Independent and tight regulation of transcriptional units in Escherichia coli via the LacR/O, the TetR/O and AraC/I1-I2 regulatory elements. *Nucleic Acids Res*, **25**, 1203-1210.

Salgado, H., Gama-Castro, S., Peralta-Gil, M., Diaz-Peredo, E., Sanchez-Solano, F., Santos-Zavaleta, A., Martinez-Flores, I., Jimenez-Jacinto, V., Bonavides-Martinez, C., Segura-Salazar, J., Martinez-Antonio, A. and Collado-Vides, J. (2006) RegulonDB (version 5.0): Escherichia coli K-12 transcriptional regulatory network, operon organization, and growth conditions. *Nucleic Acids Res*, **34**, D394-397.

Sambrook, J. and Russell, D.W. (2001) *Molecular cloning : a laboratory manual*. Cold Spring Harbor Laboratory Press, Cold Spring Harbor, N.Y.

Setsukinai, K., Urano, Y., Kakinuma, K., Majima, H.J. and Nagano, T. (2003) Development of novel fluorescence probes that can reliably detect reactive oxygen species and distinguish specific species. *J Biol Chem*, **278**, 3170-3175.

Touati, D., Jacques, M., Tardat, B., Bouchard, L. and Despied, S. (1995) Lethal oxidative damage and mutagenesis are generated by iron in delta fur mutants of Escherichia coli: protective role of superoxide dismutase. *J Bacteriol*, **177**, 2305-2314.

Whitlock, M.C. (2005) Combining probability from independent tests: the weighted Z-method is superior to Fisher's approach. *J Evol Biol*, **18**, 1368-1373.

Figure Captions

Supplementary Figure 1. **Significantly upregulated functional pathways following gyrase inhibition.**
Shown are upregulated functional groups following gyrase inhibition by norfloxacin and CcdB, as a function of time. Based on Gene Ontology classifications, statistical significance of functional groups composed of genes whose expression was significantly upregulated was calculated. Relative scale is given for each perturbation.

Supplementary Figure 2. **Significantly downregulated functional pathways following gyrase inhibition.**
Shown are downregulated functional groups following gyrase inhibition by norfloxacin and CcdB, as a function of time. Based on Gene Ontology classifications, statistical significance of functional groups composed of genes whose expression was significantly downregulated was calculated. Relative scale is given for each perturbation.

Supplementary Figure 3. **Phenotypic response of and hydroxyl radical generation by norfloxacin-resistant *E. coli***
We studied the growth behavior and hydroxyl radical generating potential of two *E. coli* strains, RFS289 (*gyrA111*) and KL317 (*gyrA17*), with norfloxacin resistance-conferring mutations in DNA gyrase. (A) Log change in colony forming units per mL (CFU/mL) of norfloxacin-treated *E. coli* strains RFS289 (blue triangles, solid line) and KL317 (red triangles, solid line) (mean +/- s.d.). Also shown is growth of untreated RFS289 (red circles, dashed line) and KL317 (blue circles, dashed line). (B) Hydroxyl radical formation was measured using the dye, HPF, following norfloxacin treatment. Shown are representative flow cytometer-measured fluorescence population distributions of RFS289 cells at time zero (grey) and at 6 hours (blue), and of KL317 cells at time zero (black) and at 6 hours (red). Also shown, in inset, are representative population distributions of untreated cells (both strains) at time zero and 6 hours.

Supplementary Figure 4. **Phenotypic response to gyrase inhibition of Δ*fur E. coli* overexpressing Fur.**
We studied the growth behavior of Δ*fur E. coli* overexpressing the iron regulatory transcription factor, Fur. Expression of Fur was induced by addition of 1mM IPTG. Shown is the log change in colony forming units per mL (CFU/mL, mean +/- s.d) of norfloxacin-treated cells (wildtype, black triangles; Δ*fur*, red triangles; Δ*fur* + Fur overexpression, blue triangles).

Supplementary Figure 5. **Fur derepression by iron chelation and superoxide response induction by paraquat.**
We monitored Fur iron regulon derepression following *o*-phenanthroline treatment and induction of the superoxide response following paraquat treatment using promoter-reporter gene constructs. These events could thus be monitored by measuring green fluorescent protein expression at single-cell resolution using a flow cytometer. These data are intended to establish the maximum expression from the respective constructs. (A) Shown are representative fluorescence population distributions of *o*-phenanthroline-treated wildtype cells at time zero (grey), 3 hours (blue) and 6 hours (red). An increase in fluorescence from our engineered pL(furO)-GFP construct is indicative of derepression of the Fur repressor protein. (B) Shown are representative fluorescence population distributions of paraquat-treated wildtype cells at time zero (grey), 3 hours (blue) and 6 hours (red). An increase in fluorescence from our pSoxS-GFP construct is indicative of SoxR oxidation by superoxide and induction of the superoxide response.

Supplementary Figure 6. **DNA damage, superoxide and iron regulatory sensor responses to gyrase inhibition.**
We monitored the occurrence of DNA damage, oxidative damage and Fur iron regulon derepression, following norfloxacin treatment **(A,C,E)** or CcdB expression **(B,D,F)**, using engineered sensor constructs. DNA lesion formation **(A,B)**, iron-sulfur cluster breakdown by superoxide **(C,D)** and iron misregulation **(E,F)**, respectively, could thus be monitored by measuring green fluorescent protein expression at single-cell resolution using a flow cytometer. Shown are representative fluorescence population distributions

of wildtype cells at time zero (grey) and of wildtype (black), Δ*atpC* (blue) and Δ*iscS* (brown) cells at 6 hours. The inset shows representative control fluorescence population distributions of untreated (norfloxacin) or uninduced (CcdB) wildtype, Δ*atpC* and Δ*iscS* cells at 6 hours.

Supplementary Figure 7. **Phenotypic response of deletion mutants to gyrase inhibition.**

Log change in colony forming units per mL (CFU/mL) of BW25113 *E. coli* deletion mutants (mean +/- s.d.). Growth of deletion mutants was compared to (A) wildtype cells treated with norfloxacin (250ng/mL; grey triangles, solid line) or expressing CcdB (grey squares, dashed line). Growth curves for all untreated knockout strains are shown for comparison purposes and are representative of growth in the absence of norfloxacin or CcdB. Survival data for treated samples are represented as mean ± SEM. (B) Survival of Δ*recA* cells (untreated, light blue circles, dotted line; drug, light blue triangles, solid line; toxin, light blue squares, dashed line). (C) Survival of Δ*atpA* cells (green squares, solid line), Δ*atpB* cells (yellow squares, solid line), Δ*atpC* cells (red squares, solid line), *ΔatpF* cells (blue triangles, solid line), and Δ*atpG* cells (red circles, solid line). (D) Survival of Δ*sodB* cells (untreated, red circles, dotted line; drug, red triangles, solid line; toxin, red squares, dashed line). (E) Survival of Δ*tonB* (untreated, yellow circles, dotted line; drug, yellow triangles, solid line; toxin, yellow squares, solid line) and Δ*fur* cells (untreated, green circles, dotted line; drug, green triangles, solid line; toxin, green squares, dashed line). (F) Survival of norfloxacin-treated Δ*iscR* cells (open triangles, dashed line), Δ*iscA* cells (filled squares, thick solid line), Δ*iscU* cells (open sqaures, thick solid line), and Δ*sufS* cells (X's, dashed line). (G) Survival of norfloxacin-treated Δ*soxS* cells (open circles, thick solid line) and Δ*sodA* (black squares, solid line).

Supplementary Figure 8. **Increased generation of ATP following gyrase inhibition.**

Using a firefly luciferase-based assay, we measured the ATP generated by gyrase-inhibited wildtype *E. coli*. (A) Gyrase inhibitor-induced ATP generation. Moles of ATP were determined for untreated wildtype cells (black triangles), CcdB-expressing wildtype cells (grey squares) and norfloxacin-treated wildtype cells (grey triangles). Moles of

ATP values were calculated by comparison to standard curve. (B) Moles of ATP per cell were calculated for untreated wildtype cells (black triangles), CcdB-expressing wildtype cells (grey squares) and norfloxacin-treated wildtype cells (grey triangles) by dividing moles of ATP by CFU/mL values.

Supplementary Figure 9. **BW25113 wildtype time course response of sensor constructs and HPF to norfloxacin.**
We monitored the occurrence of (**A**) DNA damage, (**B**) Fur iron regulon derepression, and (**C**) oxidative damage using engineered sensor constructs, and (**D**) hydroxyl radical formation using the dye, HPF, following norfloxacin treatment with 250ng/mL. Shown are representative flow cytometer-measured fluorescence population distributions of wildtype, BW25113, cells at time zero (black), 1 hour (blue), 2 hours (green), 3 hours (red), 4 hours (light blue), 5 hours (gray), and 6 hours (pink) after addition of norfloxacin.

Supplemental Figure 10. **Baseline measurements (time zero) with the sensor constructs of BW25113 mutant strains prior to gyrase inhibitor treatment.**
Representative baseline measurements of wildtype (black), Δ*atpC* (blue), Δ*fur* (green), Δ*iscS* (brown), Δ*sodB* (red), and Δ*recA* (light blue) with the DNA damage sensor prior to treatment with (A) norfloxacin or (D) CcdB expression, with the superoxide response sensor prior to treatment with (B) norfloxacin or (E) CcdB expression, and with the Fur derepression sensor prior to treatment with (C) norfloxacin or (F) CcdB expression.

Supplementary Figure 11. **Hydroxyl radicals are formed following gyrase inhibition.**
Hydroxyl radical formation was measured using the dye, HPF, following norfloxacin treatment (A) or CcdB expression (B). Shown are representative flow cytometer-measured fluorescence population distributions of wildtype cells at time zero (grey) and of wildtype (black), Δ*atpC* (dark blue), Δ*fur* (green), Δ*iscS* (brown), Δ*recA* (light blue) and Δ*sodB* (red) cells at 6 hours. The inset shows representative control fluorescence population distributions of untreated (norfloxacin) or uninduced (CcdB) wildtype, Δ*atpC*, Δ*fur*, Δ*iscS*, Δ*recA* and Δ*sodB* cells at 6 hours.

Supplemental Figure 12. **Baseline measurements (time zero) with HPF of BW25113 mutant strains prior to gyrase inhibitor treatment.**
Representative baseline measurements of wildtype (black), Δ*atpC* (blue), Δ*fur* (green), Δ*iscS* (brown), Δ*sodB* (red), and Δ*recA* (light blue) with the hydroxyl radical detecting dye HPF prior to treatment with (A) norfloxacin or (B) CcdB expression.

TABLE S4. List of bacterial strains and plasmids used in this study

Strain or plasmid	Relevant genotype	Source or reference
***E. coli* K-12 strains**		
BW25113	*lacI*^{q} *rrnB*$_{T14}$ Δ*lacZ*$_{WJ16}$ *hsdR514* Δ*araBAD*$_{AH33}$ Δ*rhaBAD*$_{LD78}$	Baba T., *et al*
BW25113 Δ*atpA*	BW25113 *atpA*::Kan^{r}	Baba T., *et al*
BW25113 Δ*atpB*	BW25113 *atpB*::Kan^{r}	Baba T., *et al*
BW25113 Δ*atpC*	BW25113 *atpC*::Kan^{r}	Baba T., *et al*
BW25113 Δ*atpF*	BW25113 *atpF*::Kan^{r}	Baba T., *et al*
BW25113 Δ*atpG*	BW25113 *atpG*::Kan^{r}	Baba T., *et al*
BW25113 Δ*fur*	BW25113 *fur*::Kan^{r}	Baba T., *et al*
BW25113 Δ*iscA*	BW25113 *iscA*::Kan^{r}	Baba T., *et al*
BW25113 Δ*iscR*	BW25113 *iscR*::Kan^{r}	Baba T., *et al*
BW25113 Δ*iscS*	BW25113 *iscS*::Kan^{r}	Baba T., *et al*
BW25113 Δ*iscU*	BW25113 *iscU*::Kan^{r}	Baba T., *et al*
BW25113 Δ*recA*	BW25113 *recA*::Kan^{r}	Baba T., *et al*
BW25113 Δ*sdhB*	BW25113 *sdhB*::Kan^{r}	Baba T., *et al*
BW25113 Δ*sodA*	BW25113 *sodA*::Kan^{r}	Baba T., *et al*
BW25113 Δ*sodB*	BW25113 *sodB*::Kan^{r}	Baba T., *et al*
BW25113 Δ*soxS*	BW25113 *soxS*::Kan^{r}	Baba T., *et al*
BW25113 Δ*sufS*	BW25113 *sufS*::Kan^{r}	Baba T., *et al*
BW25113 Δ*tonB*	BW25113 *tonB*::Kan^{r}	Baba T., *et al*
BW25113 Δ*sdhB*	BW25113 *sdhB*::Kan^{r}	Baba T., *et al*
DKΔ*atpC*	BW25113 *atpC*	This study
DKΔ*fur*	BW25113 *fur*	This study
DKΔ*iscS*	BW25113 *iscS*	This study
DKΔ*recA*	BW25113 *recA*	This study
DKΔ*sdhB*	BW25113 *sdhB*	This study
DKΔ*sodB*	BW25113 *sodB*	This study
DKΔ*tonB*	BW25113 *tonB*	This study
RFS289	Δ(*araBAD-leu*)*498*, Δ(*codB-lacI*)*3*, λ^{-}, *gyrA111*(*NalR*), *relA1*, *thi-1*	Yale Stock Center
KL317	*Leu-40*, *lacZ90*(Oc), *pyr-42*, *gyrA17*(NalR), *rpsL143*(strR)	Yale Stock Center

Plasmids		
pRR-CcdB	*ccdB*-expressing riboregulator plasmid, Kan^r	This study; Isaacs F., *et al*; Lutz H., *et al*
pFur-G	*gfpmut3b*-expressing plasmid with engineered iron regulatory promoter, Amp^r	This study; Lutz H., *et al*
pLex-G	*gfpmut3b*-expressing plasmid with engineered DNA damage promoter, Amp^r	This study; Lutz H., *et al*
pSox-G	*gfpmut3b*-expressing plasmid with native *soxS* promoter, Amp^r	This study
PIscR-G	*gfpmut3b*-expressing plasmid with native *iscR* promoter, Amp^r	This study

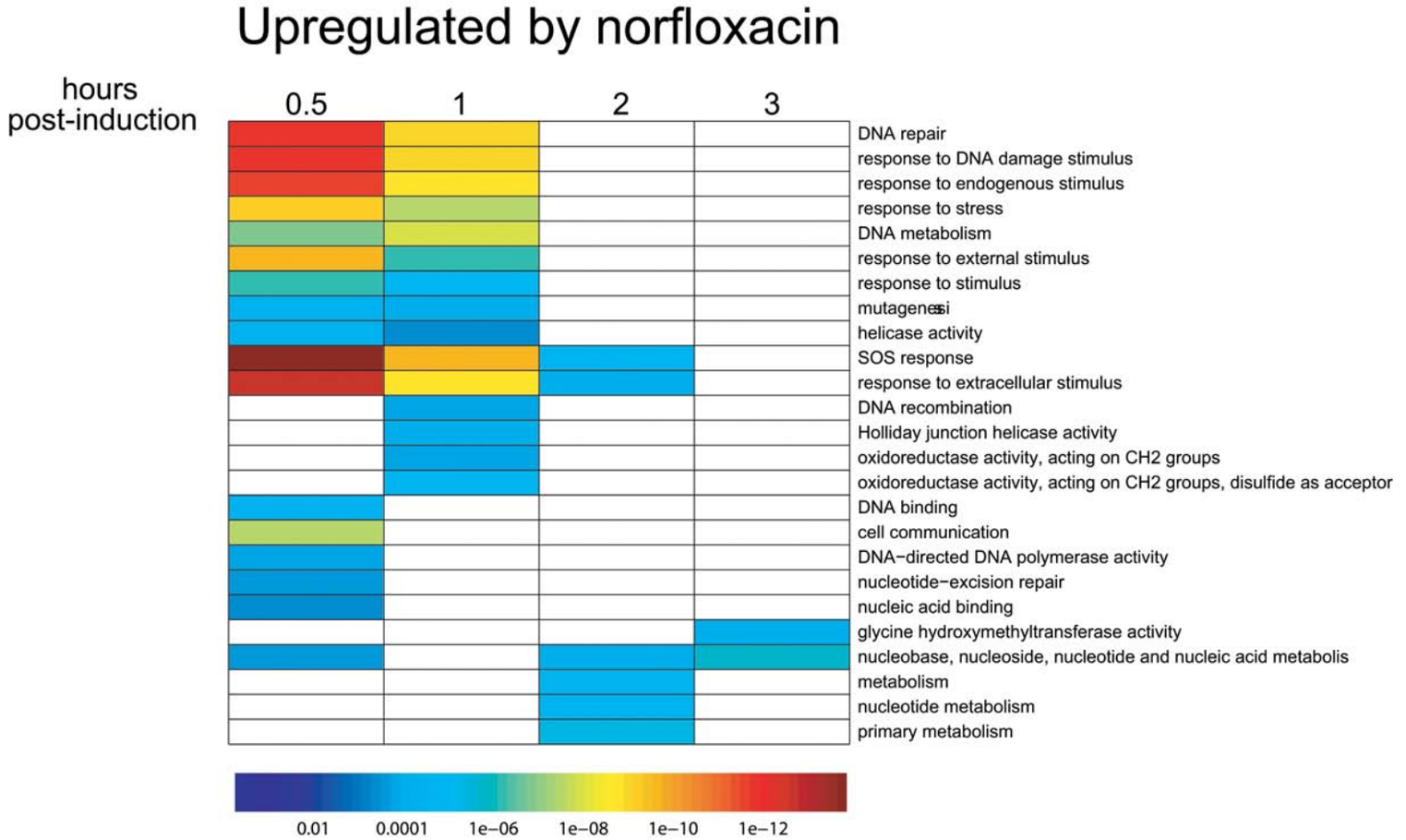

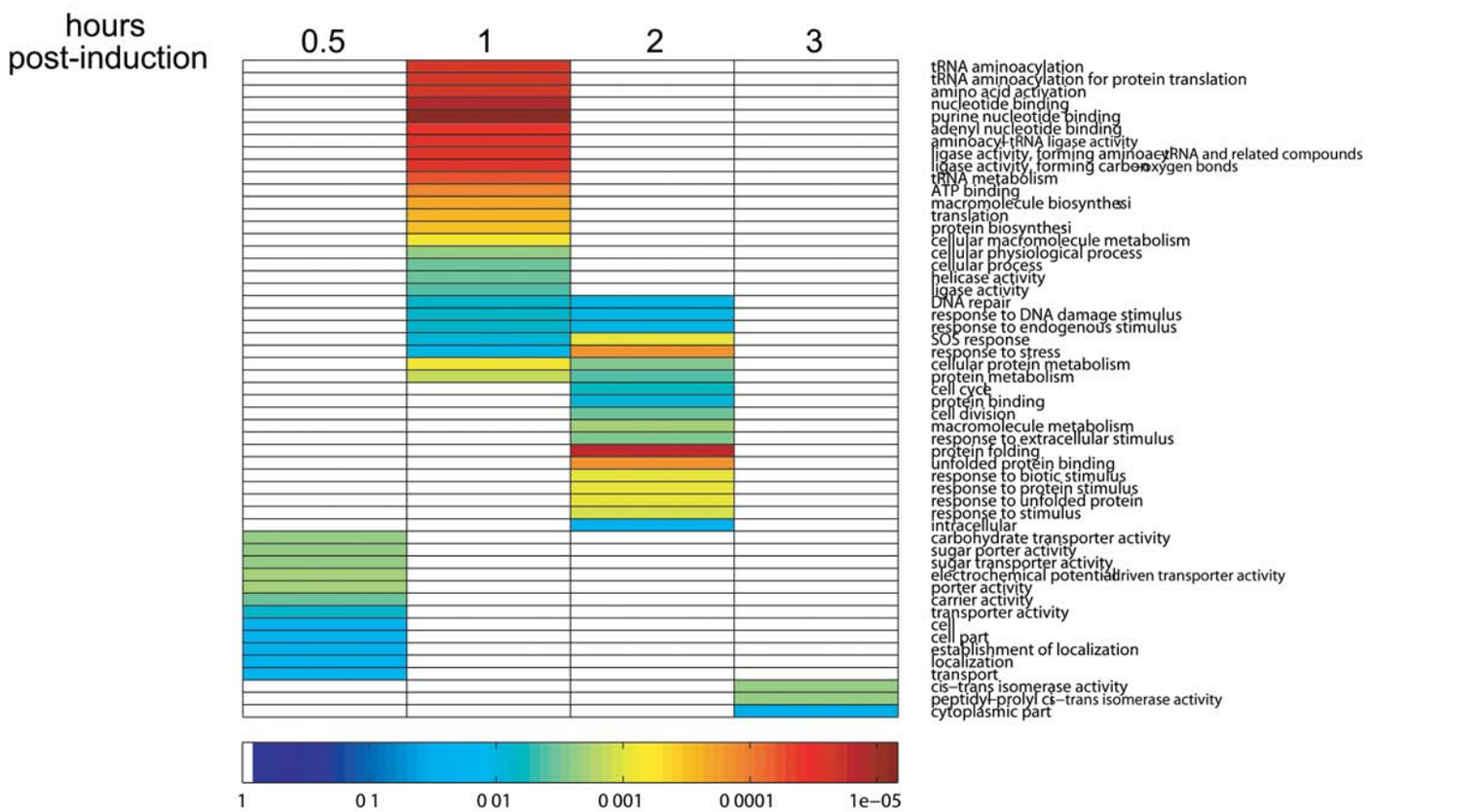

Supplementary Figure 1

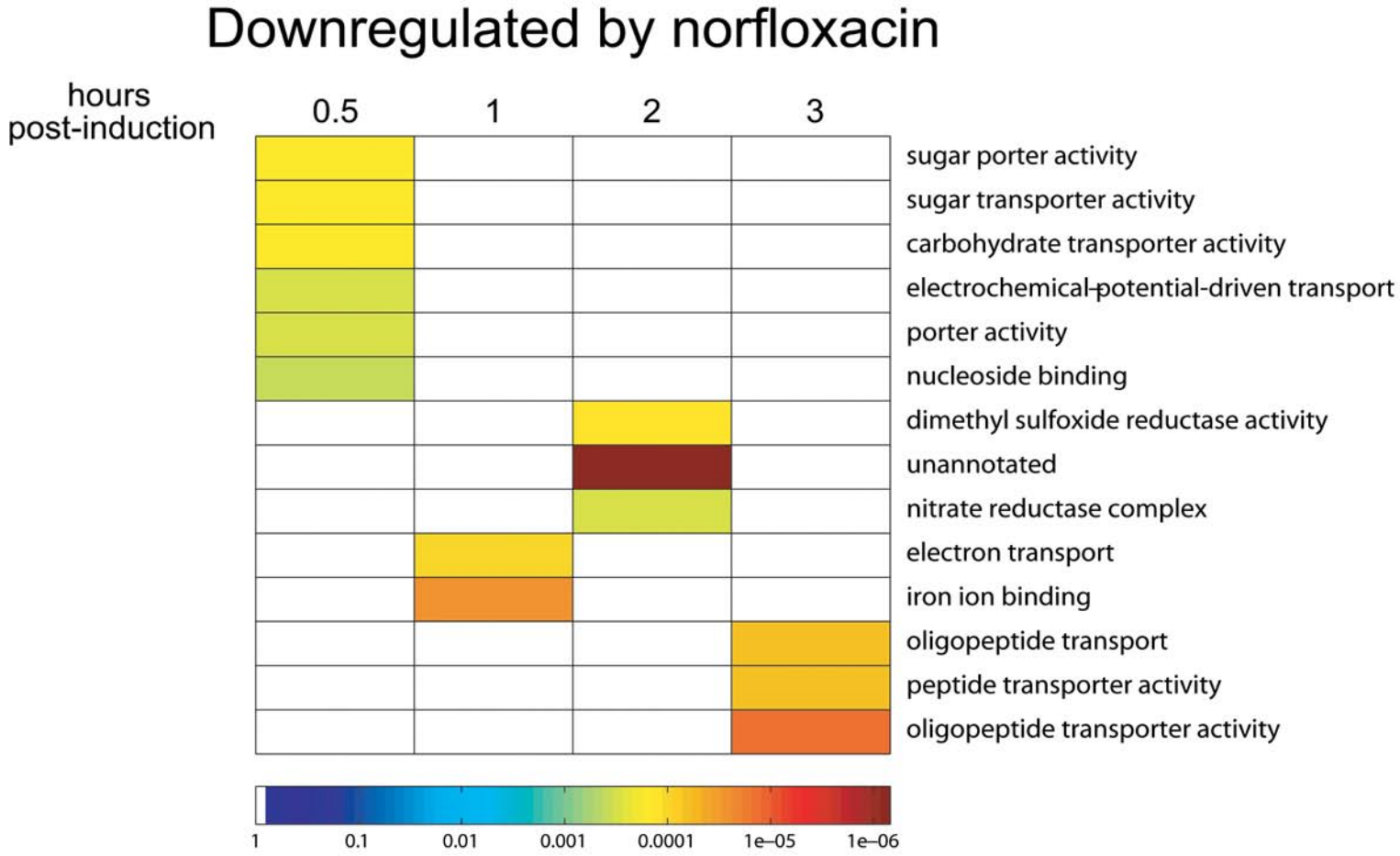

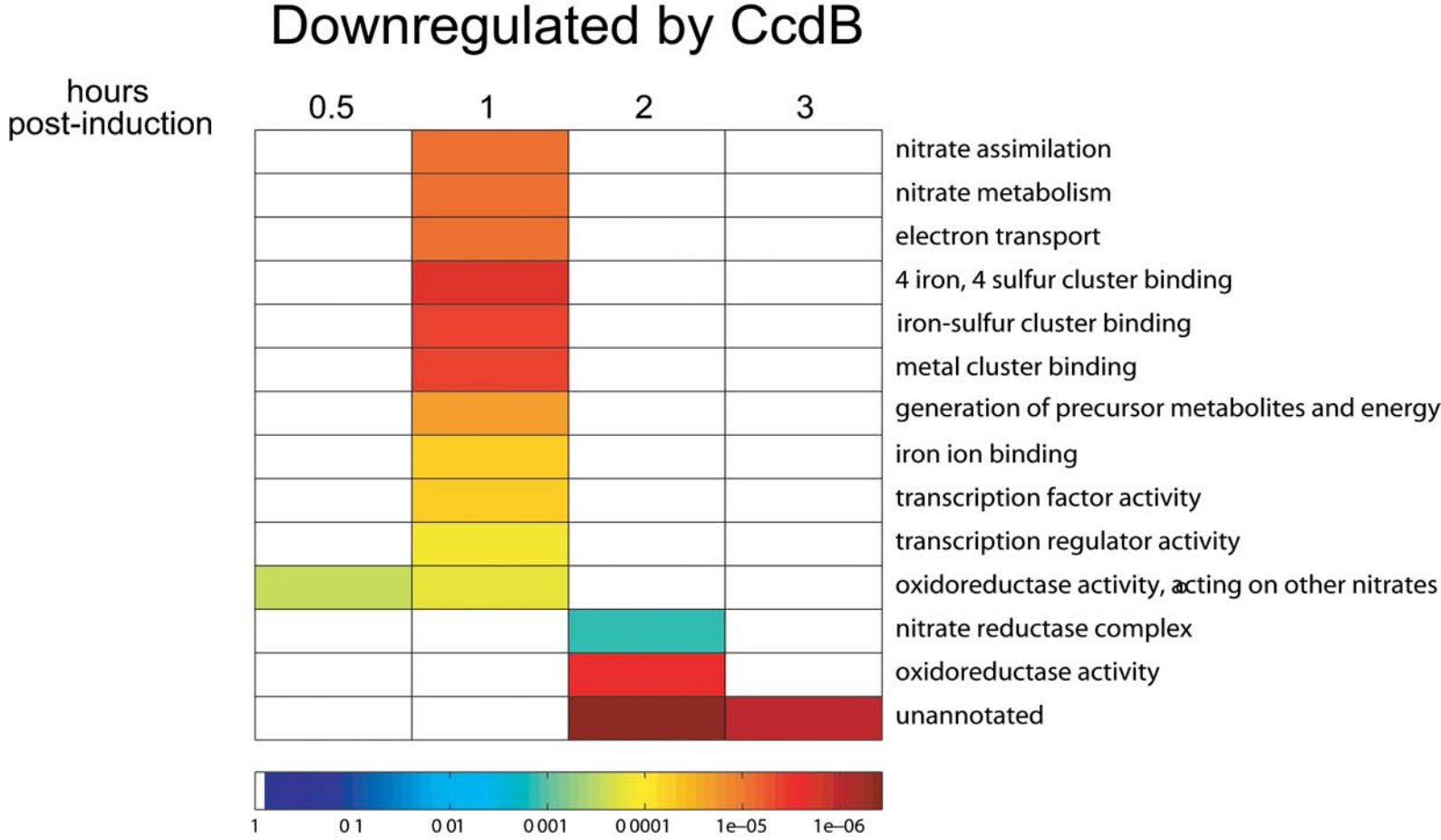

Supplementary Figure 2

A

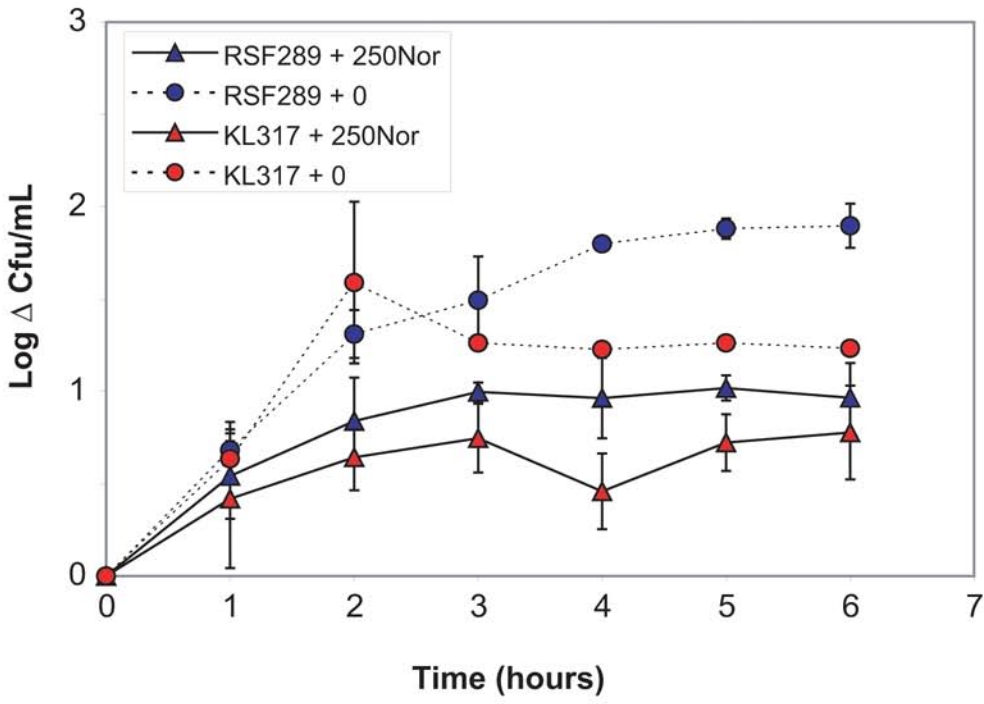

B

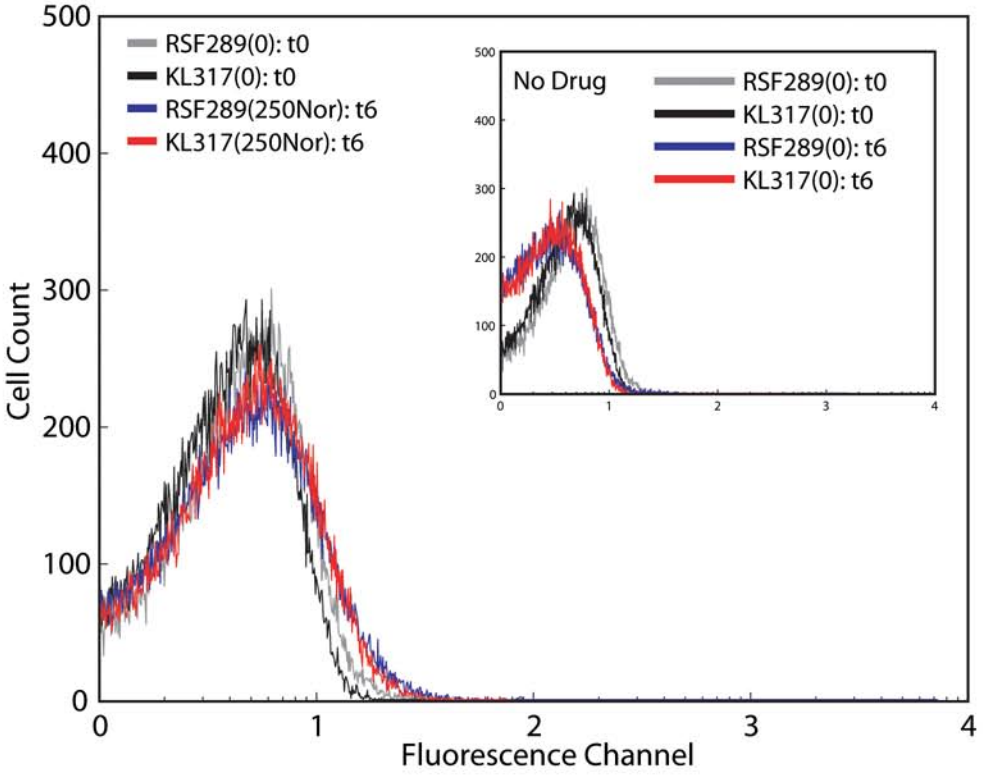

Supplementary Figure 3

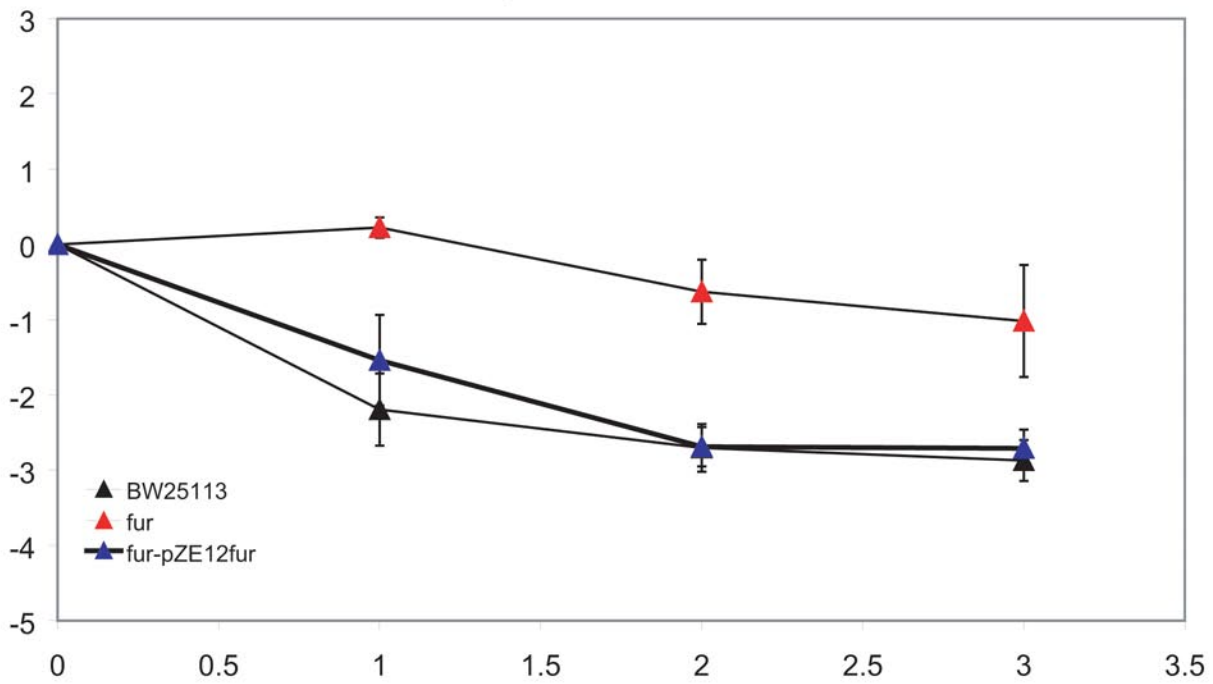

Supplementary Figure 4

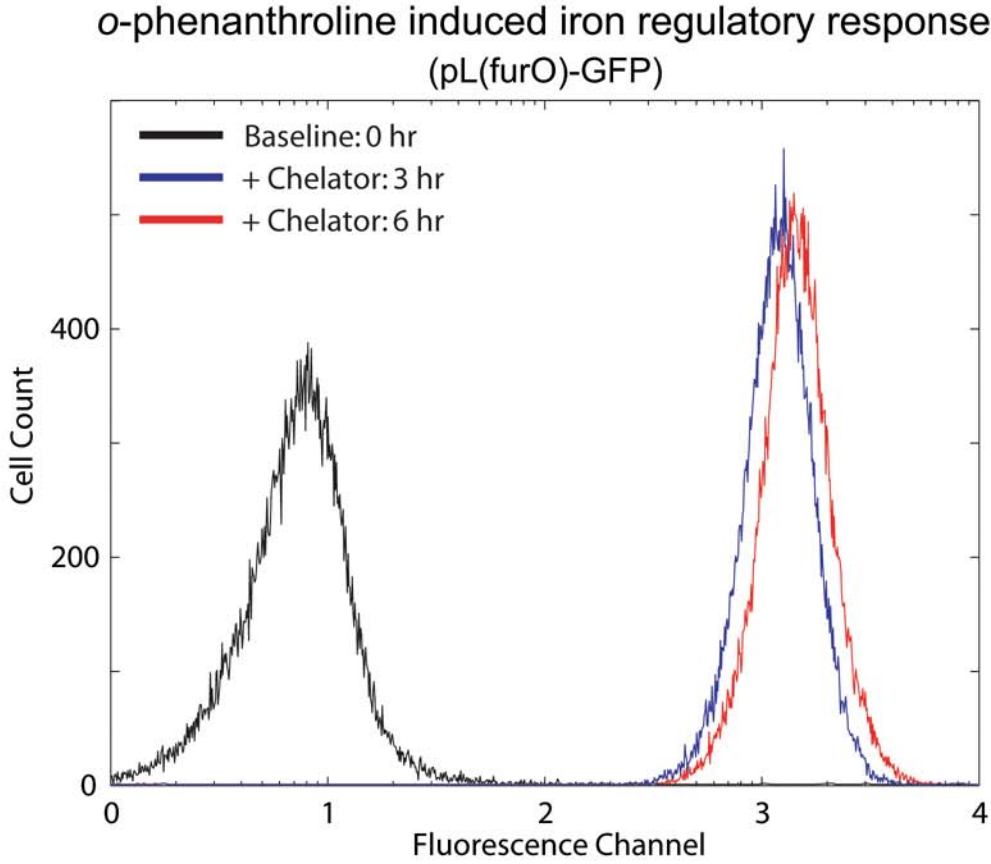

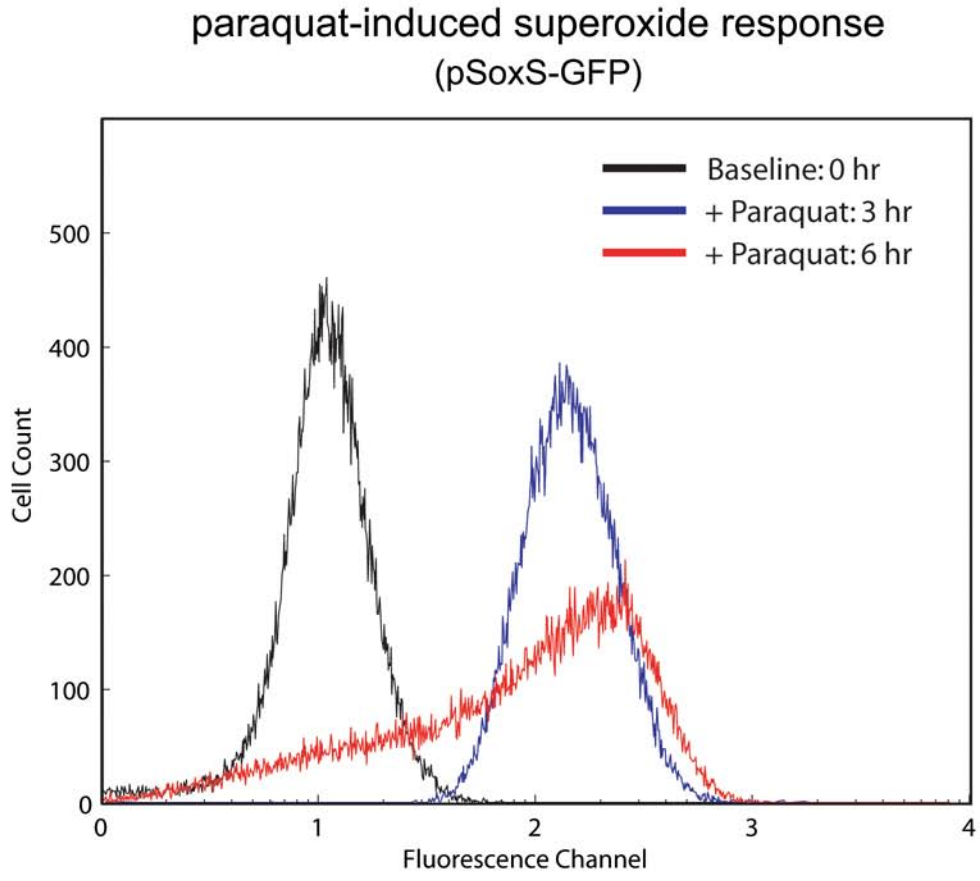

Supplementary Figure 5

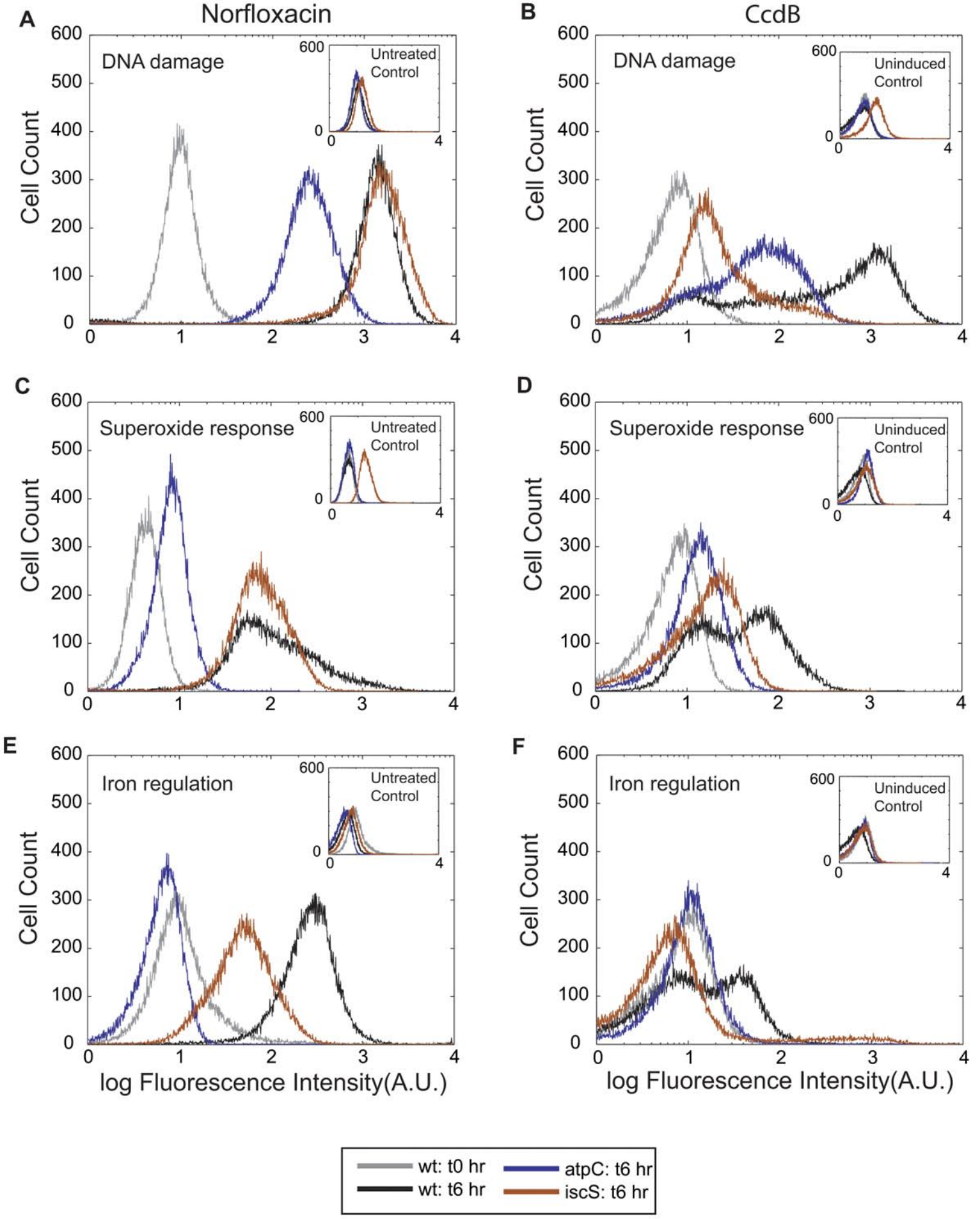

Supplementary Figure 6

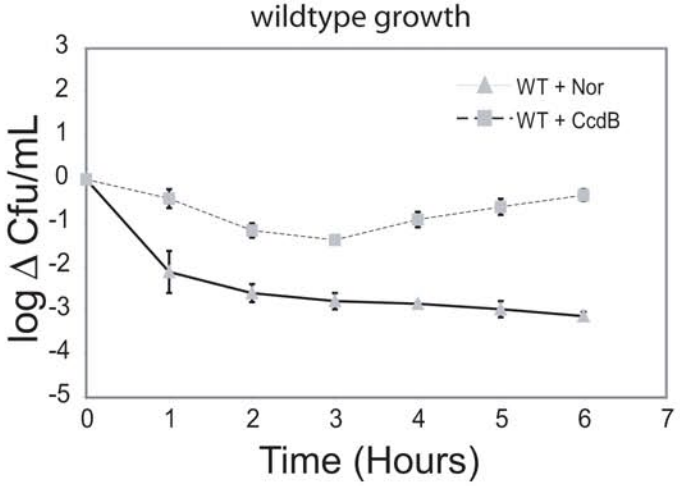

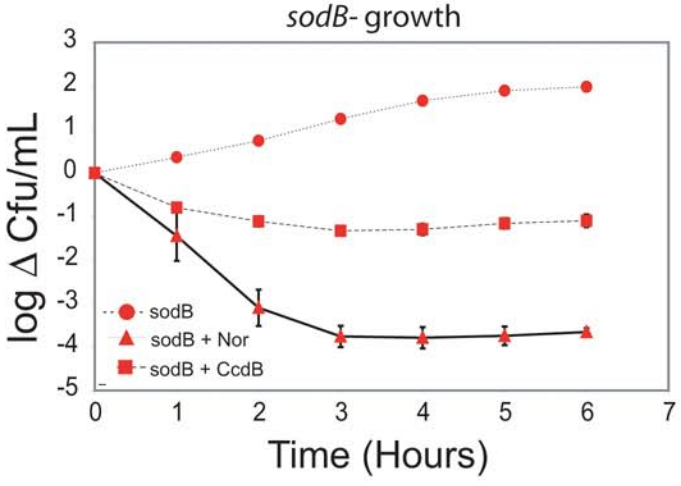

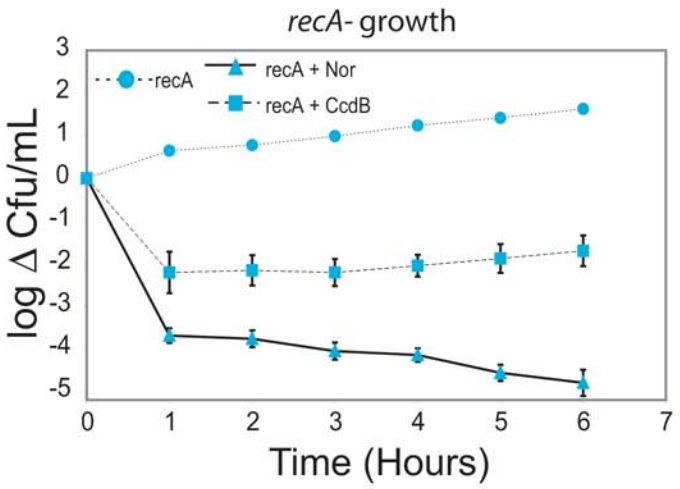

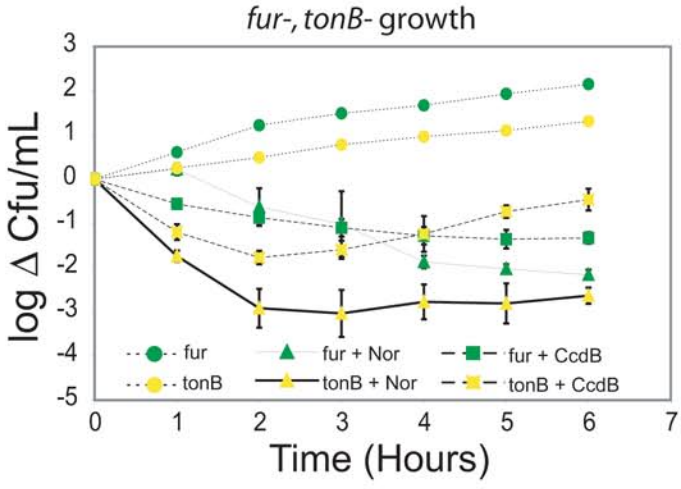

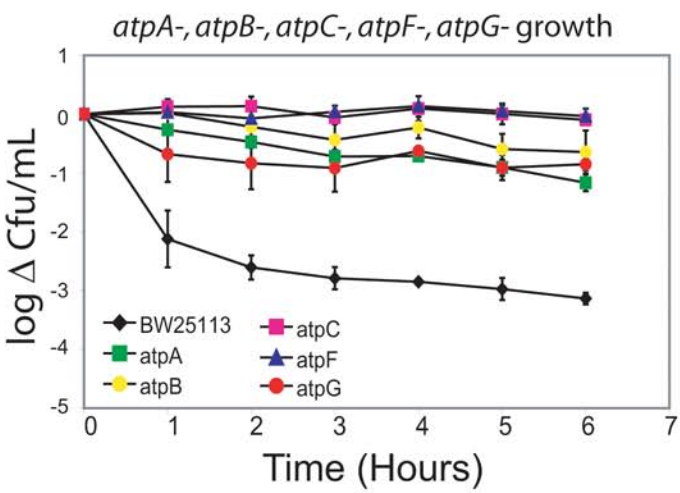

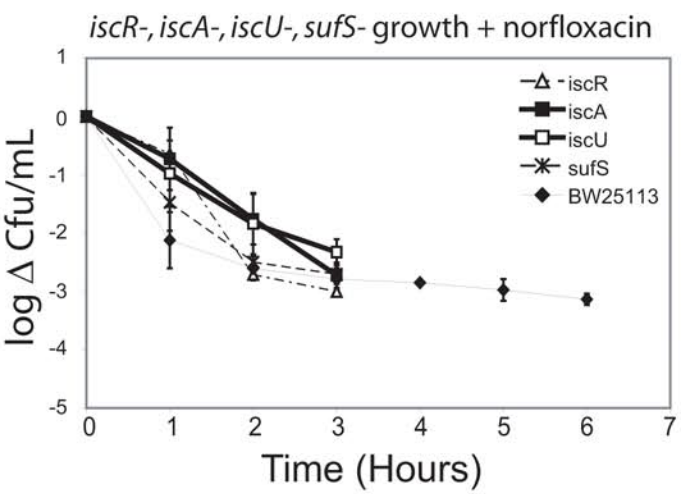

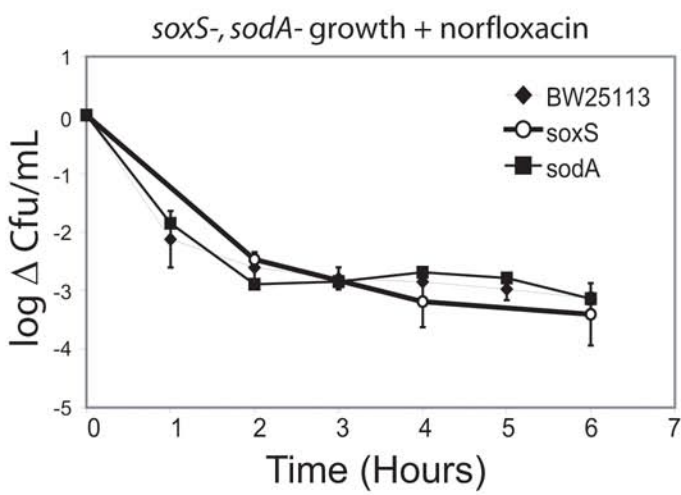

Supplementary Figure 7

A

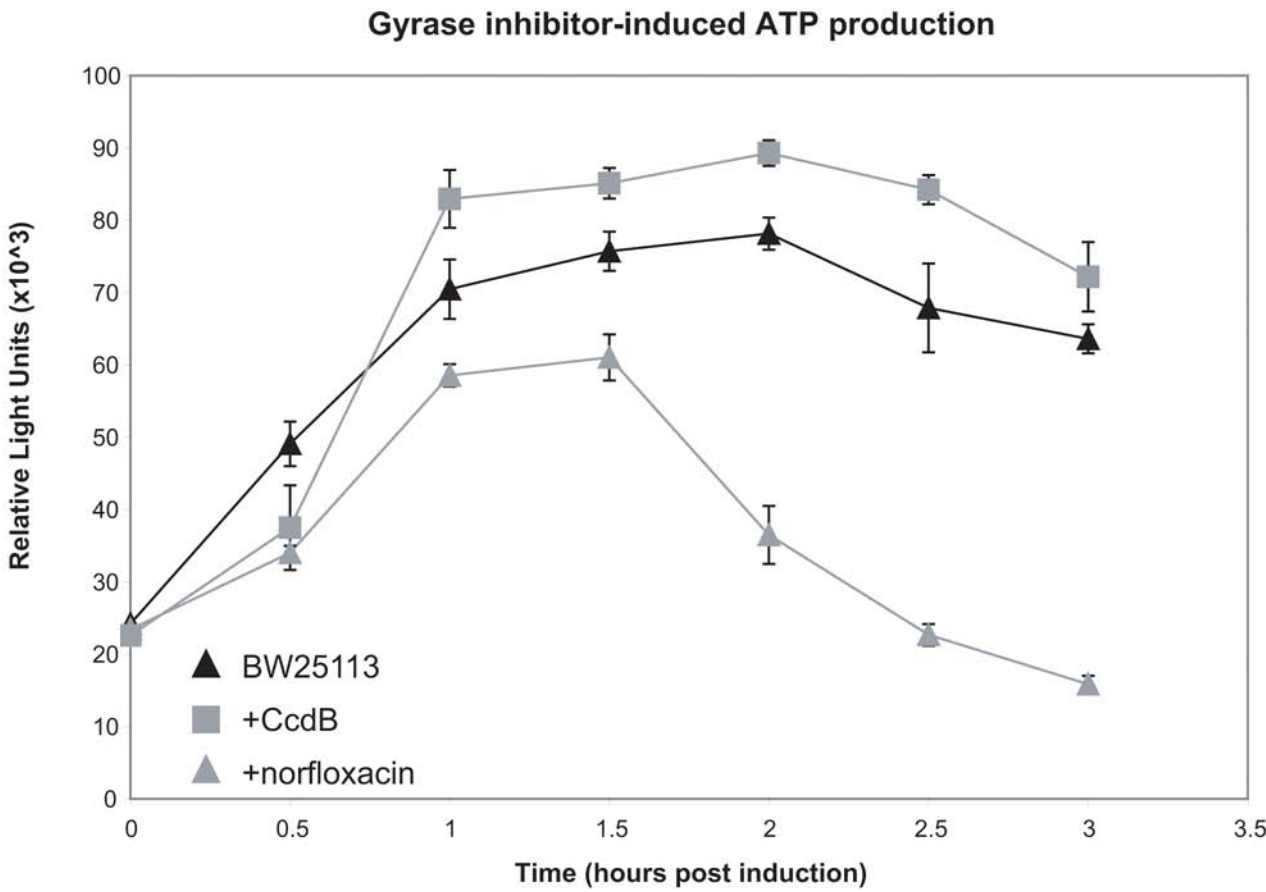

B

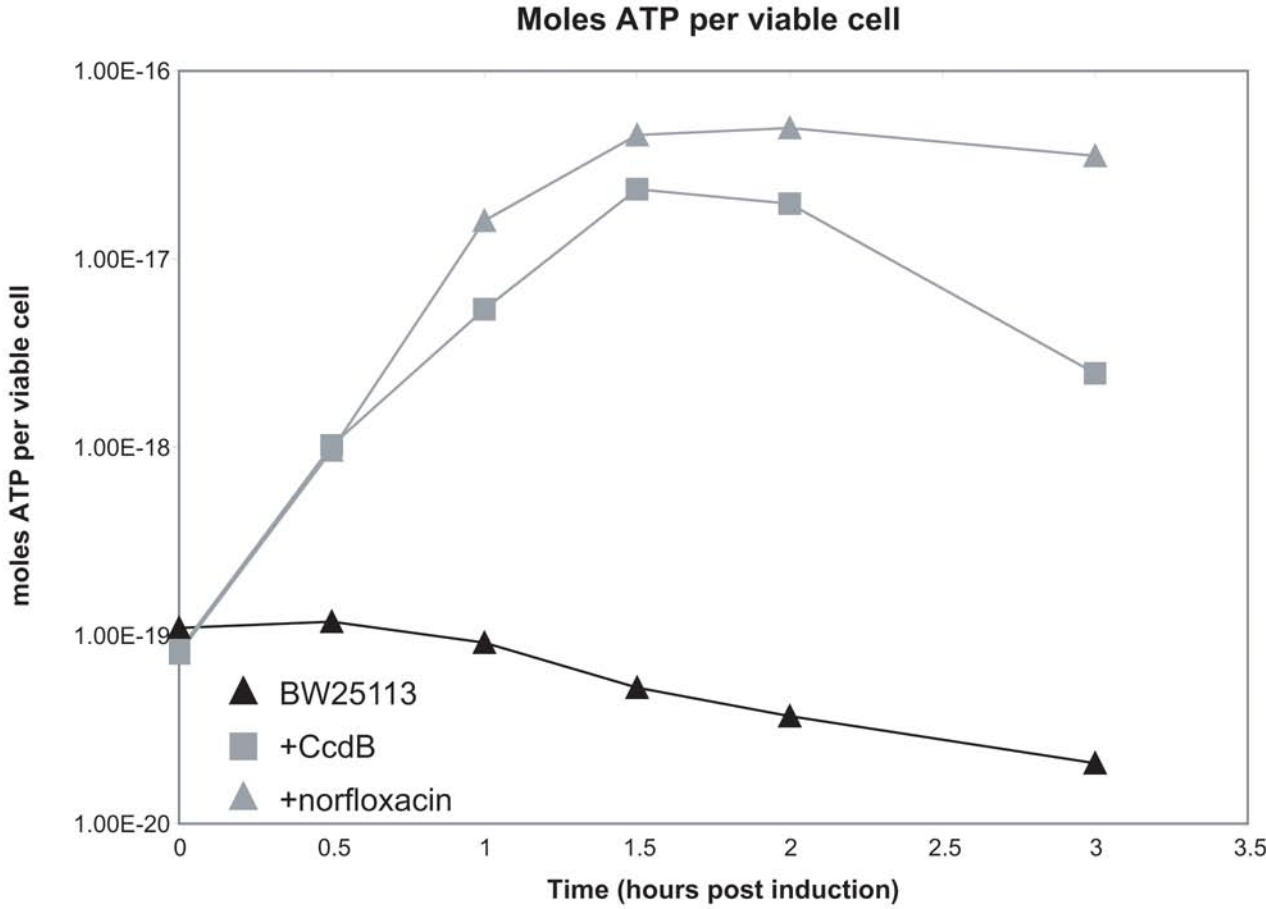

Supplementary Figure 8

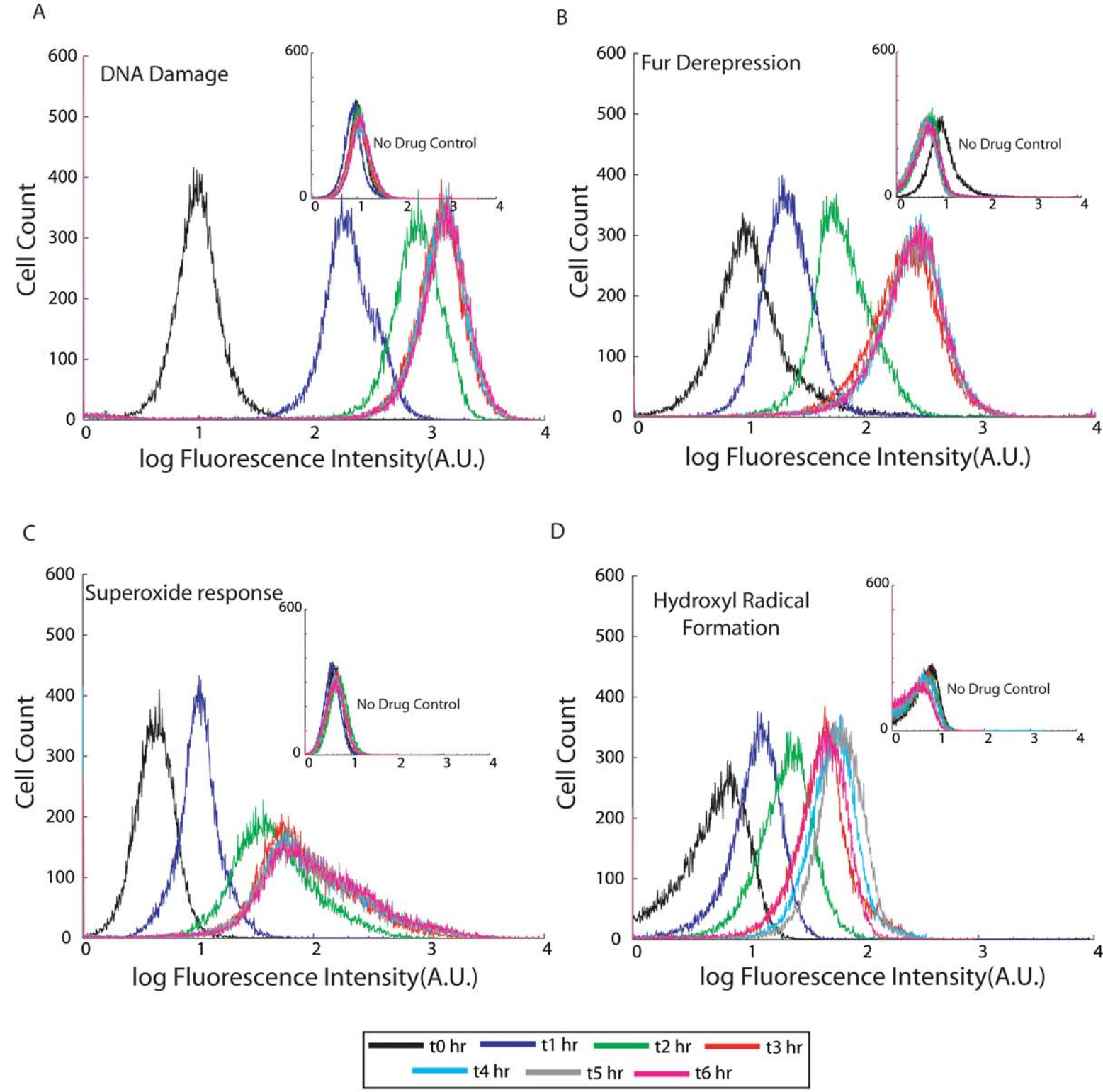

Supplementary Figure 9

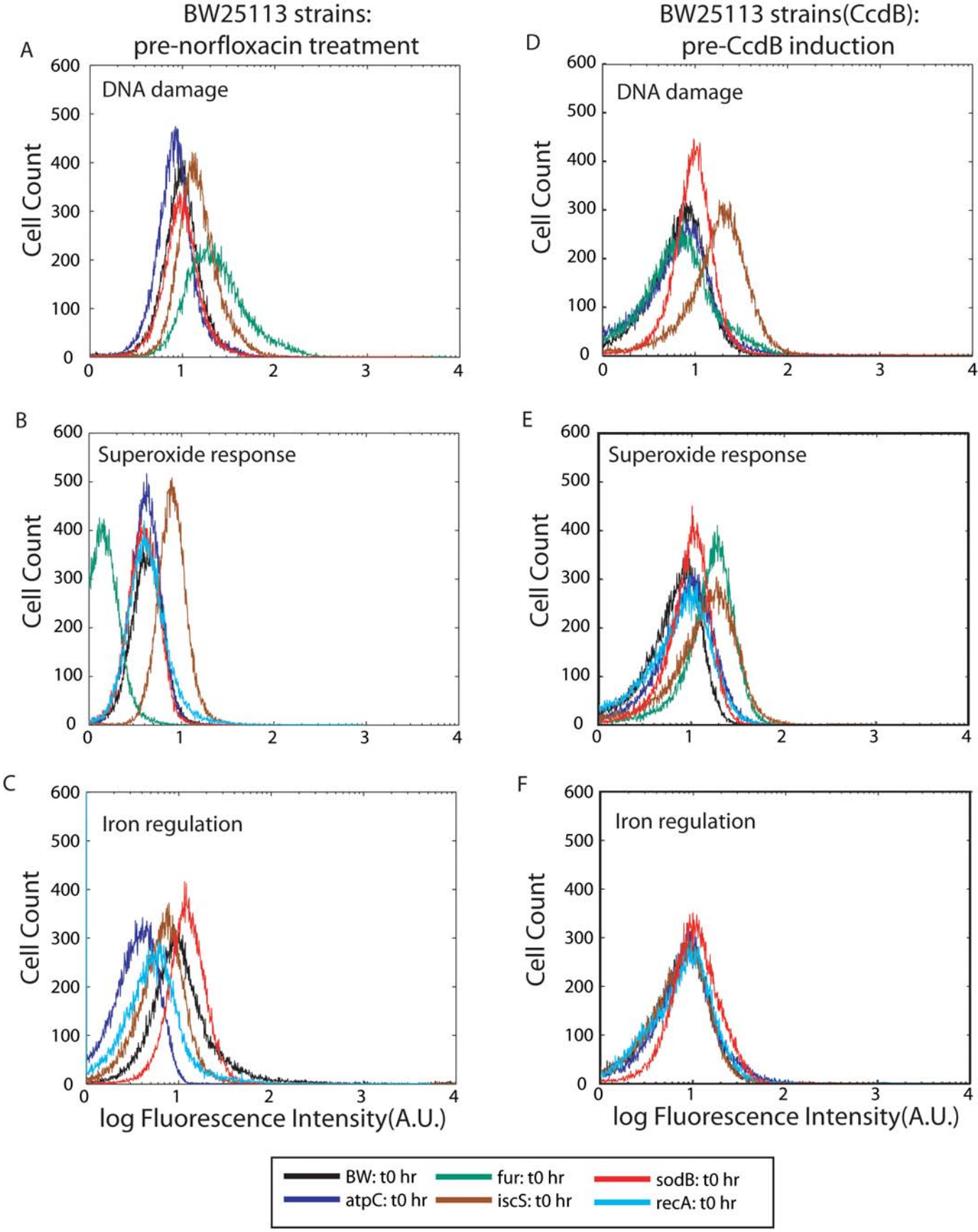

Supplementary Figure 10

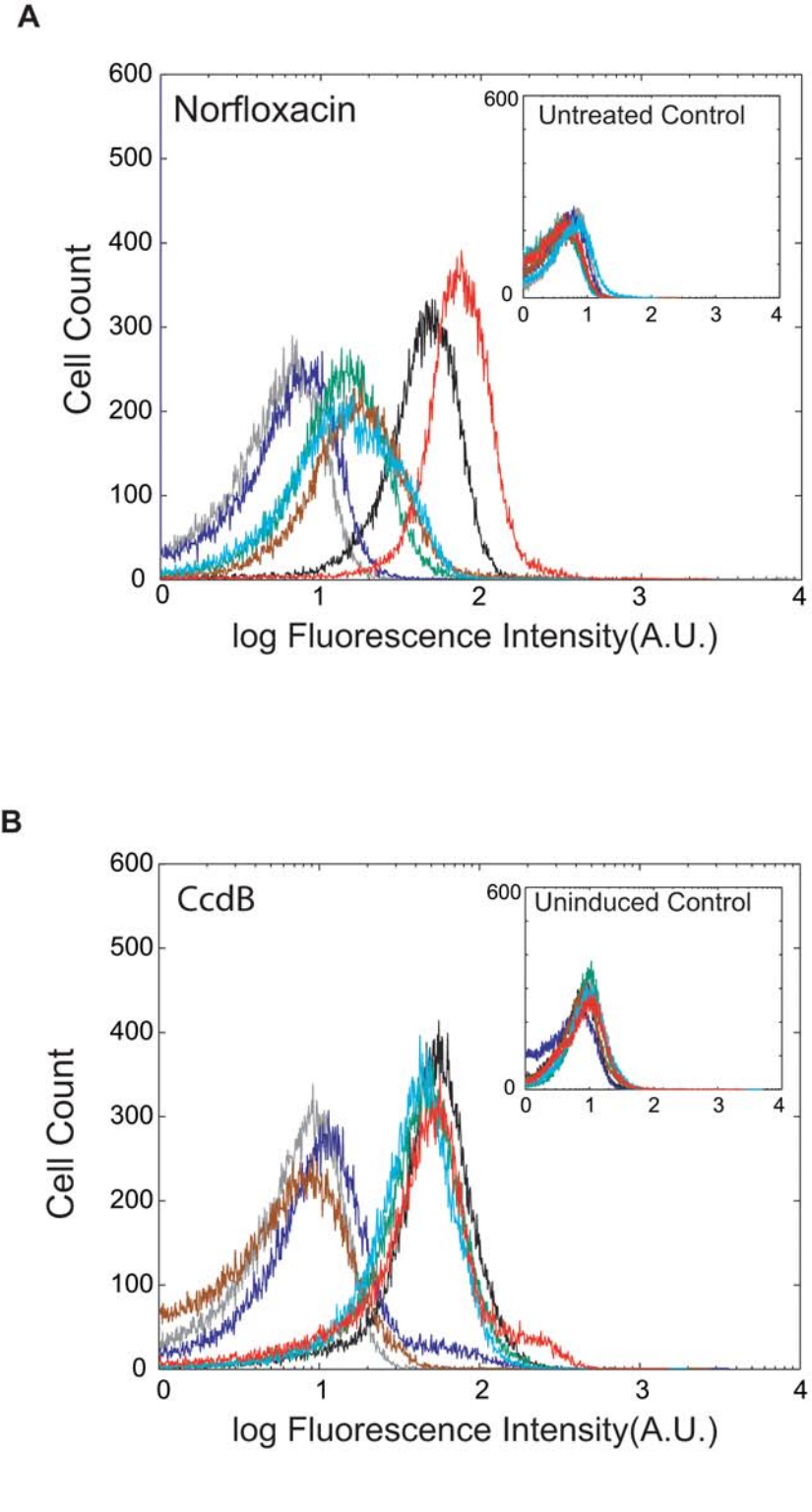

Supplementary Figure 11

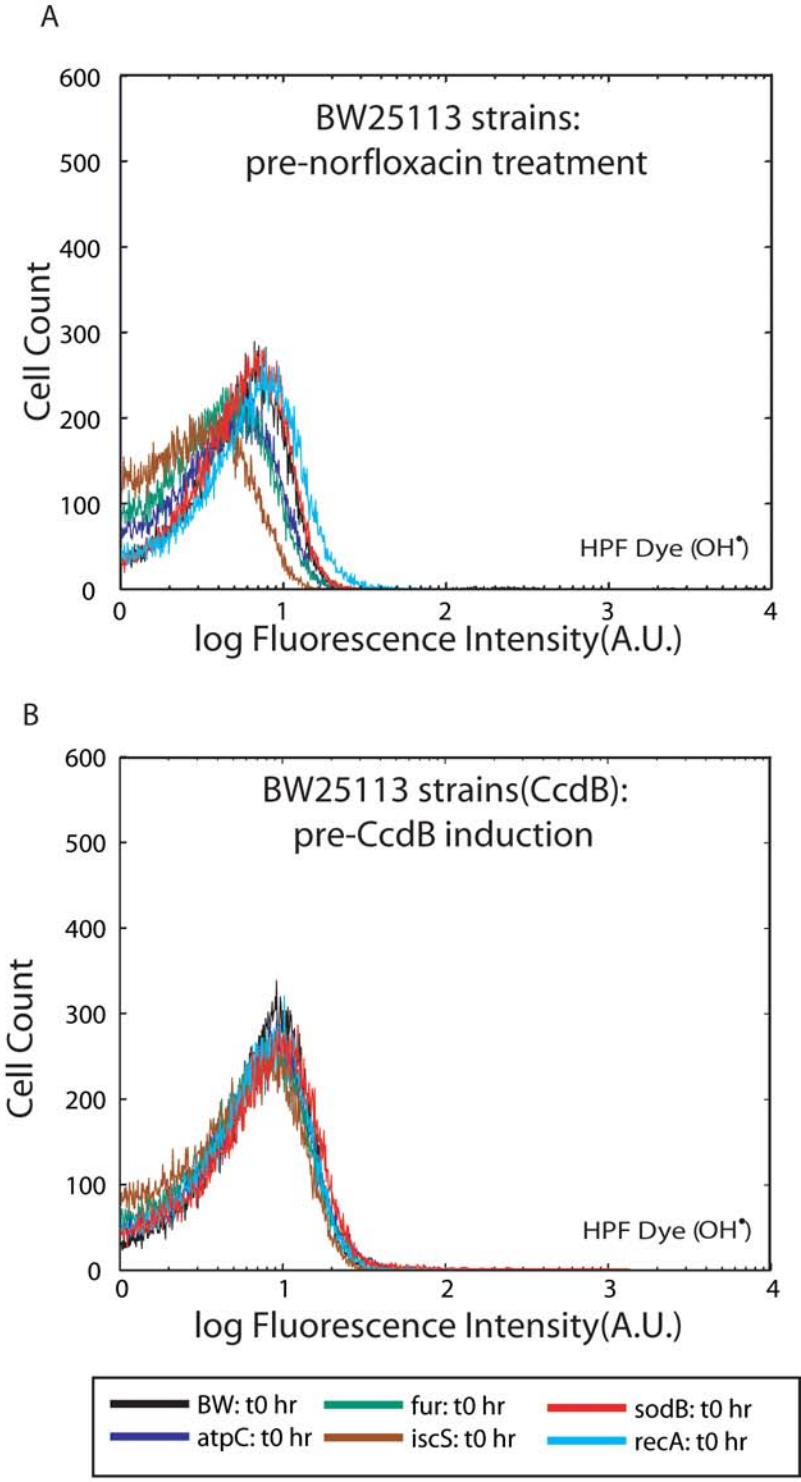

Supplemental Figure 12